広島大学学位請求論文

# Structure of Aliphatic Compounds and its Aqueous Solutions Investigated by Soft X-ray Spectroscopy

# 軟 X 線分光による脂肪族化合物および水溶液の構造研究

2022 年

広島大学理学研究科

化学専攻

山村　涼介

# 目　次

1.主論文

**Structure of Aliphatic Compounds and its Aqueous Solutions Investigated by Soft X-ray Spectroscopy**

（軟 X 線分光による脂肪族化合物および水溶液の構造研究）

山村　涼介

2.公表論文

(1) pH dependence of aqueous oxalic acid observed by X-ray absorption and emission spectroscopy
R. Yamamura, T. Suenaga, M. Oura, T. Tokushima, and O. Takahashi
Chem. Phys. Lett.　738 (2020) 136895.

(2) Identification of Valence Electronic States Reflecting the Hydrogen Bonding in Liquid Ethanol
R.　Yamamura,　K. Yamazoe, J. Miyawaki, Y. Harada, and O. Takahashi
J. Phys. Chem. B 126 (2022) 1101.
Supplementally cover picture

(3) Interpretation of the x-ray emission spectra of liquid water through temperature and isotope dependence
Osamu Takahashi, Ryosuke Yamamura, Takashi Tokushima, and Yoshihisa Harada
Phys. Rev. Lett., 128 (2022) 086002

3.参考論文

(1) Kinetics of "Melting" of Sucrose Crystals
A. Toda, R. Yamamura, K. Taguchi, T. Fukushima, and H. Kaji
Cryst. Growth Des. 18 (2018) 2602.

(2) Photoemission from the gas phase using soft x-ray fs pulses: an investigation of the space-charge effects
A. Verna, G. Stefani, F. Offi, T. Gejo, Y. Tanaka, K. Tanaka, T. Nishie, K. Nagaya, A. Niozu, R. Yamamura, T. Suenaga, O. Takahashi, H. Fujise, T. Togashi, M. Yabashi and M. Oura
New J. Phys. 22 (2020)123029.

(3) Fragmentation pathways of methylbenzoate cations following core excitation: Theoretical approach using graph theory
N. Futamata, R. Yamamura, D. T. Ha, and O. Takahashi
Chem. Phys. Lett., 766 (2021) 138316.

(4) Dissociation and ionization dynamics of CF3I and CH3I molecules via pump-and-probe experiments using soft x-ray free-electron laser
T. Gejo, T. Nishie, T. Nagayasu, K. Tanaka, Y. Tanaka, A. Niozu, K. Nagaya, R. Yamamura, N. Futamata, T. Suenaga, O. Takahashi, T. Togashi, S. Owada, H. Fujise, A. Verna, M. Yabashi, and M. Oura
J. Phys. B: At. Mol. Opt. Phys., 54 (2021)144004.

# 主論文

Contents

# Chapter 1

# General introduction

## 1-1 Spectroscopy in liquid structure

Compared to gases, where molecules are isolated, and solids, where molecules and atoms are regularly arranged, liquids are complex systems in which short-range interactions are at work, and the network is constantly changing dynamically. In the past, liquids were often treated as uniform models, but with the development of spectroscopy, local structure in liquid has been actively studied. Spectroscopy is the method that provides molecular-level information to get the state of individual molecules. Many spectroscopic techniques with light at various wavelengths are reported, and different information can be obtained depending on the wavelength. For example, in the range from ultraviolet (UV) to visible (Vis) light (10 - 700 nm), the information about valence band was obtained. In this thesis, we utilize soft x-rays (0.1 – 10 nm) with wavelengths shorter than UV.

## 1-2 Soft X-ray spectroscopy

Table 1-1: Binding energy of core to ionization levels [1].

| | K(1s) / eV | | K(1s) / eV |
|---|---|---|---|
| H | 13.6 | N | 409.9 |
| He | 24.6 | O | 543.1 |
| Li | 54.7 | F | 696.7 |
| Be | 111.5 | Ne | 870.2 |
| B | 188 | S | 2472 |
| C | 284.2 | Cl | 2822 |

Soft x-ray absorption (XAS) and emission (XES) spectroscopies are important tools for investigating the electronic structure of molecules, liquids, solid and surface adsorbates. Table 1-1 shows the binding energy from core levels to ionization [1]. Soft x-rays are light with wavelengths shorter than UV, but no longer than hard x-ray, and have an energy range of approximately 100-2000 eV. The energy of soft x-ray corresponds to the binding energy of the core level. Due to the involvement of the core level, XAS and XES are local and element specific spectroscopies, and can give valuable information about local molecular geometries and chemical bonding. Since soft x-ray has the absorption structure in oxygen and nitrogen, soft x-rays have a low penetration rate in materials and are easily attenuated in atmosphere. This is a reason that the soft x-ray spectroscopy is the method utilized in vacuum conditions. The liquid with higher vapor pressure, such as water, is difficult to introduce directly into the vacuum chamber compared

to solids. The method such as the use of thin films as separate between atmospheric pressure and vacuum, and liquid molecular beams, in which liquid is ejected into a vacuum through a fine nozzle, have made it possible to conduct experiments on liquid [2,3].

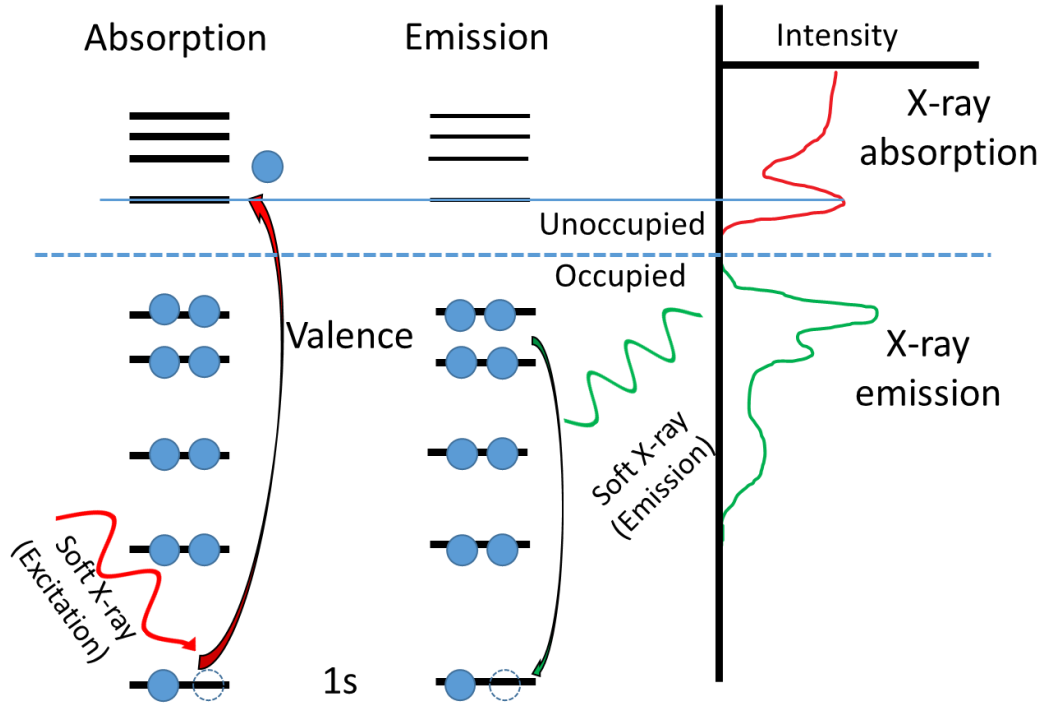


Figure 1-1: Scheme of XAS and XES.

Figure 1-1 shows the scheme of the principle of XAS and XES. When a material is irradiated with soft x-rays, electronic transitions occur in the atoms and molecules, and these transitions are more efficient when irradiated with soft x-ray of an energy corresponding to the energy difference between the core orbitals and the unoccupied orbitals, then the XAS reflects the

information of the unoccupied orbitals [4]. The unstable core hole created by the excitation of core electrons is filled again by electronic transitions, and the excess energy is emitted as soft x-ray. Since soft x-ray emission spectrum reflects the difference in energy levels between the inner shell and valence electrons, the XES obtains the information on the occupied orbitals except for the core orbital [5].

XAS and XES are similar to the commonly utilized UV spectroscopy in that they are optical absorption and emission. Compared to the UV spectroscopy, which obtains the information of molecular orbitals (MO) from unoccupied to the valence orbitals spread throughout the molecule, XAS and XES obtain the information of MOs from the unoccupied to the core orbital localized on the atom in molecules. The core electrons have very small energy dispersion because they are localized to the atoms and are not involved in chemical bonding. Due to the above characteristic of core electrons, soft x-ray spectroscopies obtain the valence electronic state, which is responsible for the properties of molecules, based on the energy levels of the core electrons. As shown in Table 1-1, the binding energy of the core electrons is large difference in each element, and the spectroscopies are element-specific method. In additions, the structure of the XAS and XES spectra vary depending on the state of the atoms in molecules.

## 1-3 Carboxylic acid solutions

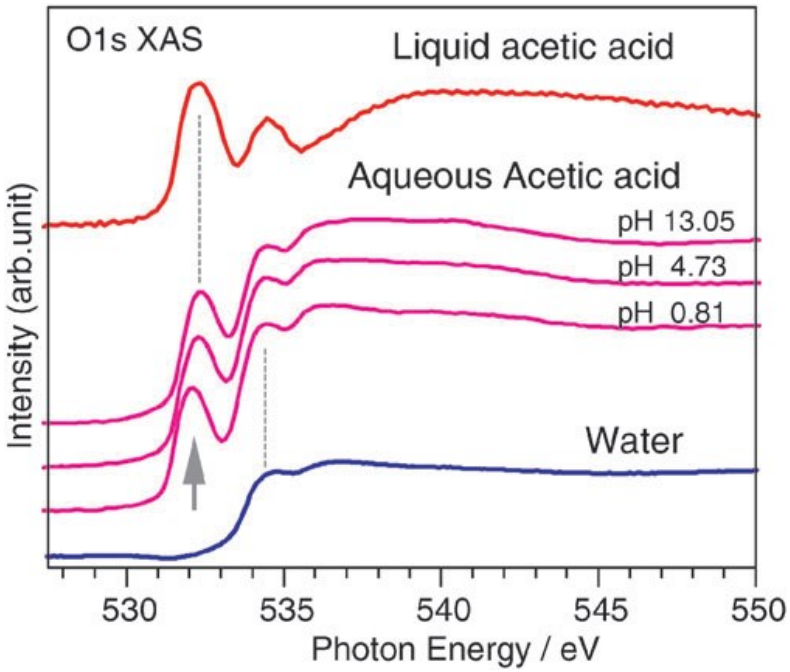


Figure 1-2: The XAS spectra of acetic acid, acetic acid aqueous solutions, and water [6]. This figure is permitted from Royal Society of Chemistry.

In liquid, molecules have different electronic state from gases and solids due to interactions from surrounding molecules. Soft x-ray spectroscopy can provide information on the electronic state in solution at the functional group level of specific molecules. Figure 1-2 shows the oxygen XAS spectra in acetic acid, aqueous acetic acid solution and water [6]. Liquid acetic acid has the absorption structure derived from the oxygen of C=O at 532 eV. Acetic acid and water still have the absorption peak structure derived from the oxygen of OH at a similar position. The peak structure of the OH in water is not as clear as that of C=O due to the effect of hydrogen bonding (h-bonding).

The XAS spectrum of aqueous acetic acid solution is a combination of the spectra of acetic acid and water. The absorption spectrum around 532 eV is absent in the absorption spectrum in water. Therefore, when an aqueous solution of acetic acid is irradiated with soft x-rays spectrum of this energy, the acetic acid molecules are mainly excited, and the electronic state of acetic acid molecules in the aqueous solutions can be selectively extracted.

As the pH changes in the aqueous acetic acid, the carboxyl group is deprotonated. Horikawa et al. reported the change of electronic state in acetic acid aqueous solutions at different pH values were observed by means of selective observations [6,7]. In these studies, isoemissive points are also observed, which implied the presence of only two populations of molecules, neutral and ionic depending on the pH. Horikawa et al. concluded that the two different forms of acetic acid in aqueous solution did not interact with each other to form new states. Thus, soft XES spectra can capture the changes in the electronic state of solutes in aqueous solutions, which called site selective XES.

However, there have been insufficient reports on site selective XES for liquid, partly because a high intensity light source is required to perform emission spectroscopy of materials in aqueous solution. In this study, dicarboxylic acids are investigated, which have two carboxyl groups and are considered to be more complex than monocarboxylic acid such as acetic acid.

Oxalic acid is the simplest dicarboxylic acid, but this molecule has several forms and coordination conformers with different stability in aqueous

solution. The chemical environment around the oxalic acid molecules leads to these different properties [8]. In aqueous solution, oxalic acid is deprotonated and can take one of three forms, neutral, anionic, or dianionic, depending on the pH value. In the neutral form, the form of oxalic acid has been suggested to have four major coordinated isomers (Figure 1-3a-d) [9-13]. The conformation of cTc is the most stable conformer in the gas phase [14-18]. Various stabilities of oxalic acid coordination isomers in the gas phase have also been reported for anionic and dianionic forms (Figure 1-3e-h) [16,19-21]. In aqueous solution, it is suggested that a different conformer is the stable[9-31]. However, the neutral and ionic coordination isomers of oxalic acid have not yet been determined. In a cluster of oxalic acid containing less than five water molecules, Hermida-Ramon et al. [22] have shown that cTt is the most stable conformer based on theoretical calculations. Buemi [31] suggested that both tCt and tTt are stable conformational isomers based on theoretical and experimental studies. Weber et al. [27] also suggested, on the basis of theoretical calculations, that tCt and tTt become increasingly important as the clusters grow larger.

In Chapter 3, we will discuss the stability of these conformers in both gas and liquid phases, and the changes in the electronic state in comparison to acetic acid using XAS and XES in experimental and theoretical aspects.

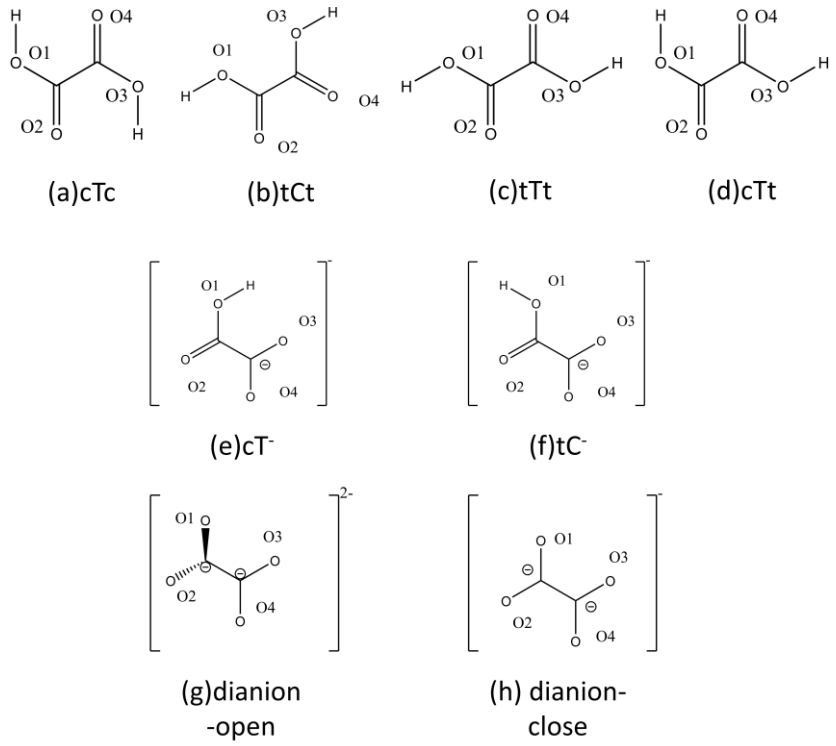


Figure 1-3: Stable conformers of oxalic acid. Labels on oxygen atoms are used in the following text. (a) – (d) neutral, (e) – (f) anionic, (g) – (h) dianionic form.

## 1-4 Model of liquid water

In the case of liquids with h-bonding, h-bonding plays a very important role for the structure. However, it has been difficult to directly observe the structure of the liquid based on h-bonding, and discussions have continued. Water is essential liquid on earth and one of the most important compounds in our lives. Despite its simple molecular structure, liquid water has many unusual physical properties [32]. Ice has a tetrahedral structure, with each water molecule connected by h-bonding. Scientists have studied liquid water using various techniques for over a century and proposed two structure model and uniform, continuous liquid model. Two structure model is proposed by Röntgen [33], revisited by Wernet et al. [34], and followed by others [32,35,36]. Uniform, continuous liquid model is proposed by Bernal and Fowler [37] and followed by researchers in a wide range of fields [3,38-41]. The interpretation of x-ray spectroscopy with respect to its sensitivity to the h-bonding structure of liquid water is controversial, although comparable experimental data have been reported by various groups [3,42,43].

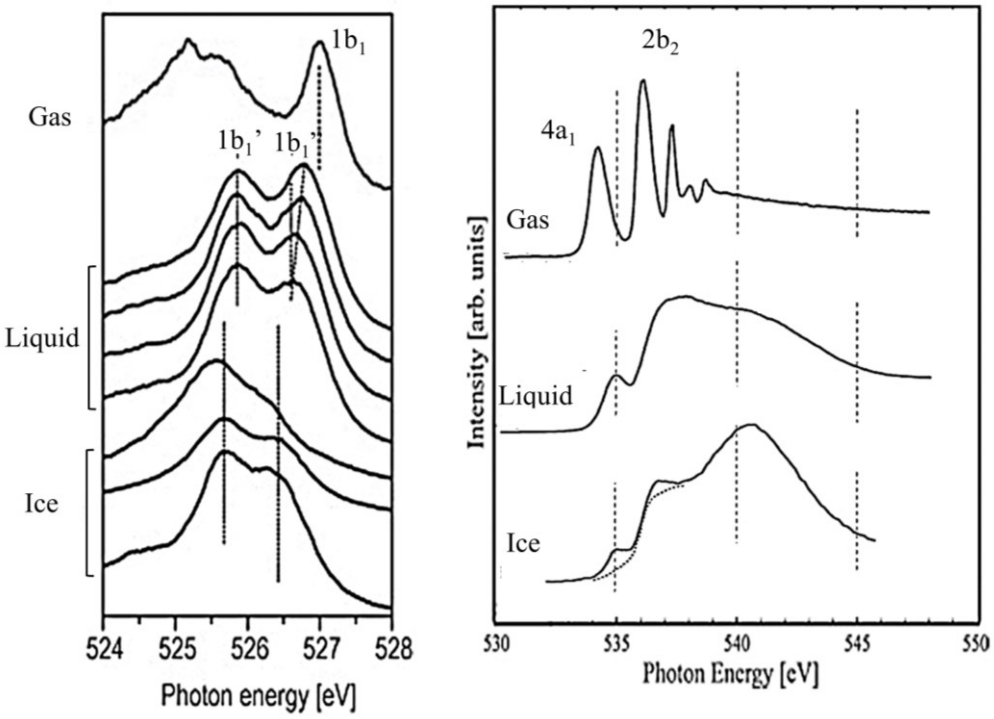


Figure 1-4: Temperature-dependent XES [3] (left) and XAS [44] (right) spectra. These figures are permitted from Elsevier.

Figure 1-4 shows the experimental XAS [44] and XES [3] spectra of gaseous, liquid and solid water. The unoccupied orbitals observed in the XAS spectra are sensitive to the surrounding environment and interactions of molecule due to the large spread of the molecular orbitals. Therefore, XAS spectra of the liquid water and ice are observed with broad peak structure compared with that of the gas phase that is greatly affected by h-bonding. The spectra in the liquid phase have a prominent structure around 540 eV due to the change in coordination number of h-bonding [34,45].

As already described in the section 1-2, the XES spectra reflects the information of molecular orbitals in the valence level. In the case of water molecular, the emission is due to the electronic transitions from three molecular orbitals assigned as $1b_1$, $3a_1$, and $1b_2$ using the irreducible representation of $C_{2v}$ point group caused by excitation of the oxygen 1s electrons [46]. However, in the XES spectra of liquid, the double peak structures were observed around 525–526 eV. The double peaks possess the same symmetry, and are assigned as $1b_1$' and $1b_1$" by adopting the symmetry symbol of orbitals used for the gas phase of water [46]. When the temperature of the water changed, the relative intensity of the two peaks changed. The intensity of $1b_1$" increases with increasing temperature and the peaks located close to water vapor, while the intensity of $1b_1$' increase at low temperature and is located to close to ice, indicating an ice-like component.

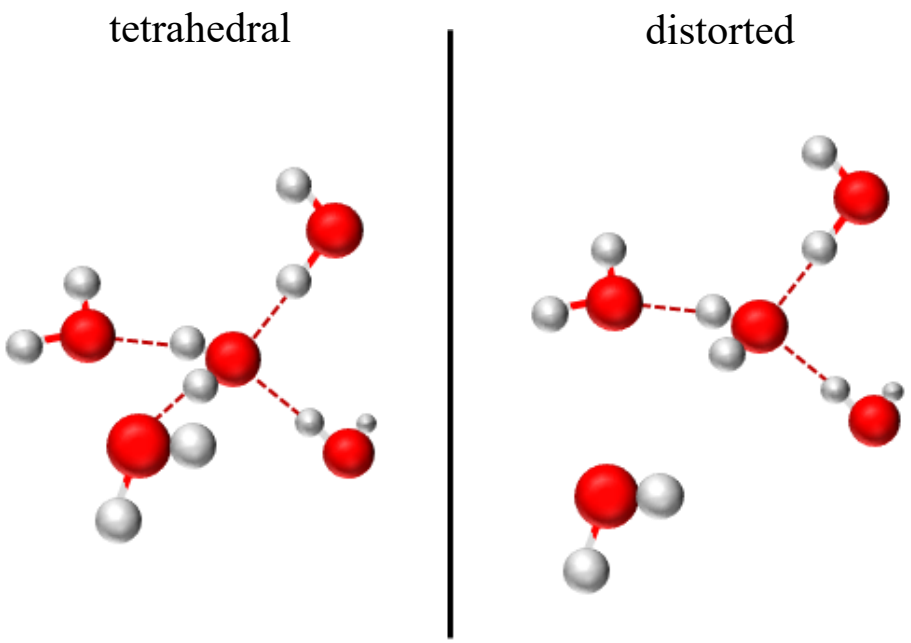


Figure 1-5: Two model structures of liquid water (left: tetrahedral, right: distorted).

A huge problem is continuing about the interpretation of XES of liquid water. Despite comparable experimental data of liquid water, several interpretations are reported. Tokushima et al. [3] reported that the double peak was interpreted to represent two different local h-bonding structures, as shown in Figure 1-5. On the other hands, Fuchs et al. [42] claimed that the double peak structure can be reproduced by using a uniform, continuous liquid model and considering ultrafast O-H bond dissociation dynamics during the lifetime of the O 1s core hole. In their opinion, both interpretations agree on the importance of h-bonding features in the liquid phase. The interpretation based on two-structure models is now associated with the

concept of low- and high-density amorphous liquids (LDL and HDL) at low temperatures [35]. Under ambient conditions, they are corresponding to different distributions of tetrahedrally coordinated water and water clusters with highly distorted or broken h-bonding. Recent reports have used the resonant inelastic x-ray scattering (RIXS) technique to discuss the dynamical effects on resonantly excited states in liquid water [47,48]. Zhovtobriukh [49] et al. reproduced the double $1b_1$ peaks in the XES spectra of liquid water by applying arbitrary sampling to molecular dynamics (MD) simulations. More recently, Shi and Tanaka [50], using x-ray scattering experiments and MD simulations, reported the existence of two local structures in liquid water. Cruzeiro et al. [51] suggested that it is impossible to unambiguously attribute the split of the $1b_1$ peak to only two specific structural arrangements of the underlying h-bonding network, although core-hole-induced dynamics were absent in their simulations. Piskulich and Thompson [52] reported the temperature dependence of the oxygen-oxygen radial distribution function (RDF) of liquid water using MD simulations.

We report the theoretical reproduction of the double $1b_1$ peak feature of XES in liquid water. Several effects, such as geometry and dynamics, were discussed to determine the shape of the XES spectra in Chapter 5.

## 1-5 Liquid ethanol

Water has two hydrogens attached to one oxygen, making it a complex molecule in terms of looking at h-bonding in liquids. Thus, we investigate ethanol, which is a molecule with a simple structure contains only one OH bond, for the h-bonding structure. Ethanol is widely used as solvents, reagents, and raw materials in many branches of industry. Ethanol may be seen as an analog of water, where one hydrogen is replaced by an ethyl group. Both systems include the h-bonding, however it does not make ethanol analogous to water, which results in a variety of structures and properties. Furthermore, it has similar properties to liquid water, where h-bonding interactions are dominant. Therefore, the differences in the physical properties of water and ethanol can be discussed by investigating the nature of h-bonding [50,53]. Ethanol molecules have a hydrophobic group and multiple heterogeneous, dynamic structures due to competition between hydrophobic interactions and intermolecular h-bonding [54-57].

The properties of liquid ethanol can be comprehensively interpreted by examining the local and cluster structures, which are the aggregates of ethanol molecules. Several experimental techniques, such as x-ray diffraction [58], neutron diffraction [59], nuclear magnetic resonance (NMR) [60], XAS [61], XES [62,63], and RIXS have been utilized [47]. Theoretically, for the O-C-C plane of an ethanol molecule, two different h-bonding configurations involving out-of-plane and in-plane lone electron pairs of excited oxygen atoms appear as two peaks in the XES [62]. It is also

important to use MD simulations to investigate the local structure and cluster structure of liquid ethanol.

In Chapter 4, XES profiles of liquid ethanol are compared experimentally and theoretically in the framework of local structural changes, using temperature as a parameter to change the interactions in the system. The temperature-induced changes in the local structure of liquid ethanol have been studied theoretically and an accurate assignment of the peaks in the XES profiles has been provided. In addition, MD simulations were used to investigate the temperature dependence of the cluster structure of liquid ethanol. Finally, the mechanism of the local structural changes in liquid ethanol with temperature was expounded to compare the experimental and simulated data.

## 1-7 Purpose and outline of this thesis

As mentioned above, the liquid state has a lot of unresolved issues, and the XAS and XES are the important tool for solving them, shown in Chapter 2. We investigate the liquid structure using theoretical and experimental methods. In Chapter 3, we conduct a combined experimental and theoretical analysis of oxalic acid. Next, we focus on h-bonding in the liquid. In Chapter 4, we discuss the h-bonding structure in liquid ethanol, which is a molecule with a simple structure which contains only one OH bond and investigate the effect of the h-bonding structure on the XES spectra. Finally, in Chapter 5, we discuss the interpretation of XES spectra of liquid water.

## References


[1] J. A. Bearden, A. F. Burr, Rev. Mod. Phys. 39 (1967) 125.

[2] T. Tokushima, Y. Harada, H. Ohashi, Y. Senba, S. Shin, Rev. Sci. Instrum. 77 (2006) 063107.

[3] T. Tokushima, Y. Harada, O. Takahashi, Y. Senba, H. Ohashi, L.G.M. Pettersson, A. Nilsson, S. Shin, Chem. Phys. Lett. 460 (2008) 387.

[4] J. Stöhr, NEXAFS spectroscopy, Springer Verlag Berlin Heidelberg 1992, 1996.

[5] J. Nordgren, G. Bray, S. Cramm, R. Nyholm, J. E. Rubensson, N. Wassdahl, Rev. Sci. Instrum. 60 (1989) 1690.

[6] Y. Horikawa, T. Tokushima, Y. Harada, O. Takahashi, A. Chainani, Y. Senba, H. Ohashi, A. Hiraya, S. Shin, Phys. Chem. Chem. Phys. 11 (2009) 8676.

[7] T. Tokushima, Y. Horikawa, Y. Harada, O. Takahashi, A. Hiraya, S. Shin, Phys. Chem. Chem. Phys. 11 (2009) 1679.

[8] A. J. Eugene, E. A. Pillar, A. J. Colussi, M. I. Guzman, Langmuir 34 (2018) 9307.

[9] E. G. Schnitzler, C. Badran, W. Jäger, J. Phys. Chem. Lett. 7 (2016) 1143.

[10] H. J. Maria, S. P. McGlynn, J. Mol. Spectrosc. 42 (1972) 177.

[11] S. E. Cabaniss, J.A. Leenheer, I. F. McVey, Spectrochim. Acta, Part A 54 (1998) 449.

[12] K. Ito, H. J. Bernstein, Can. J. Chem. 34 (2011) 170.

[13] M. Darvas, S. Picaud, P. Jedlovszky, Phys. Chem. Chem. Phys. 13 (2011) 19830.

[14] B.C. Stace, C. Oralratmanee, J. Mol. Struct. 18 (1973) 339.

[15] E. Maçôas, R. Fausto, M. Pettersson, L. Khriachtchev, M. Rasanen, J. Phys. Chem. A 104 (2000) 6956.

[16] C. Chen, S. F. Shyu, Int. J. Quantum Chem. 76 (2000) 541.

[17] A. Mohajeri, N. Shakerin, J. Mol. Struct. THEOCHEM 711 (2004) 167.

[18] M. Remko, K. R. Liedl, B. M. Rode, Journal of the Chemical Society, Perkin Transactions, Perkin Transactions 2 (1996) 1743.

[19] G. L. Hou, M. Valiev, X. B. Wang, J. Phys. Chem. A 120 (2016) 2342.

[20] D. G. Kuroda, R. M. Hochstrasser, Phys. Chem. Chem. Phys. 14 (2012) 6219.
[21] O. Kroutil, B. Minofar, M. Kabelac, J. Mol. Model. 22 (2016) 210.
[22] J. M. Hermida-Ramón, E. M. Cabaleiro-Lago, J. Rodríguez-Otero, Chemical Physics 302 (2004) 53.
[23] D. Y. Naumov, N. V. Podberezskaya, E. V. Boldyreva, A. V. Virovets, Chem. Phys. 37 (1996) 480.
[24] M. Weisser, W. Weyrich, Z. Naturforsch., A: Phys. Sci. 48 (1993) 1.
[25] V. Mohaček-Grošev, J. Grdadolnik, J. Stare, D. Hadži, J. Raman Spectrosc. 40 (2009) 1605.
[26] P. D. Godfrey, M. J. Mirabella, R. D. Brown, J. Phys. Chem. A 104 (2000) 258.
[27] K. H. Weber, F.J. Morales, F. M. Tao, J. Phys. Chem. A 116 (2012) 11601.
[28] A. Lautié, Y. Belabbes, Spectrochim. Acta, Part A 52 (1996) 1903.
[29] P. A. W. Dean, J. Chem. Educ. 89 (2012) 417.
[30] R. J. Clark, S. Firth. Spectrochim. Acta, Part A 58 (2002) 1731
[31] G. Buemi, J. Phys. Org. Chem. 22 (2009) 933.
[32] P. Gallo, K. Arnann-Winkel, C. A. Angell, M. A. Anisimov, F. Caupin, C. Chakravarty, E. Lascaris, T. Loerting, A. Z. Panagiotopoulos, J. Russo, J. A. Sellberg, H. E. Stanley, H. Tanaka, C. Vega, L. M. Xu, L. G. M. Pettersson, Chem. Rev. 116 (2016) 7463.
[33] W. C. Röntgen, Ann. Phys. 281 (1892) 91.
[34] P. Wernet, D. Nordlund, U. Bergmann, M. Cavalleri, M. Odelius, H. Ogasawara, L. A. Naslund, T.K. Hirsch, L. Ojamae, P. Glatzel, L. G. M. Pettersson, A. Nilsson, Science 304 (2004) 995.
[35] A. Nilsson, L. G. M. Pettersson, Nat. Commun. 6 (2015).
[36] P. H. Handle, T. Loerting, F. Sciortino, Proc. Natl. Acad. Sci. U.S.A. 114 (2017) 13336.
[37] J. D. Bernal, R. H. Fowler, J. Chem. Phys. 1 (1933) 515.
[38] L. J. William, C. Jayaraman, D. M. Jeffry, W. I. Roger, L.K. Michael, J. Chem. Phys. 79 (1983) 926.
[39] R. A. Marcus, J. Chem. Phys. 24 (1956) 966.
[40] G. C. Pimentel, A. L. McClellan, The Hydrogen Bond, Freeman, San

Francisco, 1960.
[41] G. N. I. Clark, C. D. Cappa, J. D. Smith, R. J. Saykally, T. Head-Gordon, Mol. Phys. 108 (2010) 1415.
[42] O. Fuchs, M. Zharnikov, L. Weinhardt, M. Blum, M. Weigand, Y. Zubavichus, M. Bar, F. Maier, J.D. Denlinger, C. Heske, M. Grunze, E. Umbach, Phys. Rev. Lett. 100 (2008) 027801.
[43] K. Yamazoe, J. Miyawaki, H. Niwa, A. Nilsson, Y. Harada, J. Chem. Phys. 150 (2019) 204201.
[44] A. Nilsson, D. Nordlund, I. Waluyo, N. Huang, H. Ogasawara, S. Kaya, U. Bergmann, L. A. Naslund, H. Ostrom, P. Wernet, K. J. Andersson, T. Schiros, L. G. M. Pettersson, J. Electron. Spectrosc. Relat. Phenom. 177 (2010) 99.
[45] J. A. Sellberg, S. Kaya, V. H. Segtnan, C. Chen, T. Tyliszczak, H. Ogasawara, D. Nordlund, L. G. M. Pettersson, A. Nilsson, J. Chem. Phys. 141 (2014).
[46] T. Tokushima, Y. Horikawa, H. Arai, Y. Harada, O. Takahashi, L. G. M. Pettersson, A. Nilsson, S. Shin, J. Chem. Phys. 136 (2012) 044517.
[47] V. d. C. Vinícius, F. Gel'mukhanov, S. Eckert, M. Iannuzzi, E. Ertan, A. Pietzsch, R.C. Couto, J. Niskanen, M. Fondell, M. Dantz, T. Schmitt, X. Lu, D. McNally, R.M. Jay, V. Kimberg, A. Föhlisch, M. Odelius, Nat. Commun. 10 (2019) 1013.
[48] V. d. C. Vinícius, I. Nina, C. C. Rafael, A. F. Daniil, R. R. Dirk, S. Viktoriia, N. Patrick, Å. Hans, P. Sergey, N. Johannes, E. Sebastian, M.J. Raphael, F. Mattis, S. Thorsten, P. Annette, F. Alexander, G.m. Faris, O. Michael, K. Victor, J. Chem. Phys. 150 (2019) 234301.
[49] I. Zhovtobriukh, N.A. Besley, T. Fransson, A. Nilsson, L.G.M. Pettersson, J. Chem. Phys. 148 (2018) 144507.
[50] R. Shi, H. Tanaka, J. Am. Chem. Soc. 142 (2020) 2868.
[51] V.W.D. Cruzeiro, A. Wildman, X. Li, F. Paesani, J. Phys. Chem. Lett. 12 (2021) 3996.
[52] A. P. Zeke, H. T. Ward, J. Chem. Phys. 152 (2020) 011102.
[53] Y. Marechal, The hydrogen bond and the water molecule: The physics and chemistry of water, aqueous and bio-media, Elsevier, 2006.
[54] A. Vrhovsek, O. Gereben, A. Jamnik, L. Pusztai, J. Phys. Chem. B 115

(2011) 13473.
[55] T. A. Dolenko, S. A. Burikov, S. A. Dolenko, A. O. Efitorov, I. V. Plastinin, V. I. Yuzhakov, S. V. Patsaeva, J. Phys. Chem. A 119 (2015) 10806.
[56] I. A. Finneran, P. B. Carroll, M. A. Allodi, G. A. Blake, Phys. Chem. Chem. Phys. 17 (2015) 24210.
[57] F. Li, Z. Men, S. Li, S. Wang, Z. Li, C. Sun, Spectrochim. Acta, Part A 189 (2018) 621.
[58] A.H. Narten, A. Habenschuss, J. Chem. Phys. 80 (1984) 3387.
[59] C.J. Benmore, Y. L. Loh, J. Chem. Phys. 112 (2000) 5877.
[60] R. Ghanghas, A. Jindal, S. Vasudevan, J. Phys. Chem. B 124 (2020) 662.
[61] R. K. Lam, J. W. Smith, R. J. Saykally, J. Chem. Phys. 144 (2016) 191103.
[62] O. Takahashi, M. P. Ljungberg, L. G. M. Pettersson, J. Phys. Chem. B 121 (2017) 11163.
[63] M. P. Ljungberg, I. Zhovtobriukh, O. Takahashi, L. G. M. Pettersson, J. Chem. Phys. 146 (2017) 134506.

# Chapter 2

# Experimental and theoretical methods

## 2-1 Experimental method

Experiments of the O 1s XES in oxalic acid aqueous solution and liquid ethanol were performed the BL17SU [1,2] and using the BL07LSU [3] HORNET station [4] at SPring-8, and all spectra were measured using a liquid flow cell with a 150 nm-thick Au-coated thin-film $Si_3N_4$ and SiC window to separate the liquid flowing at atmospheric pressure from the high vacuum region, respectively [1-4]. In the BL07LSU, the temperature can be controlled by supplying a temperature-controlled cold medium from the chiller to the water jacket of the liquid cell within an error range of 0.3°C. In the experiment of temperature dependence of liquid ethanol, the temperature was set at 241 K and 313 K. The oxalic acid aqueous solution was prepared at pH 1.1, 2.7, and 12.9 using sodium hydroxide, and the concentration was set at 0.2 M.

## 2-2 Theoretical method

### 2-2-1 Oxalic acid

To obtain the theoretical model structure of an aqueous solution of oxalic acid, we adopt the MD simulation. As a start point of calculation, the most stable conformer in solvent water was calculated with Becke, 3-parameter, and Lee‑Yang‑Parr (B3LYP) and Pople basis sets as 6-311++G(d,p) level [5-9] and the polarizable continuum model (PCM) method [10-12] were performed in this calculation implemented in GASUSSIAN09 [13]. Then, a NVT (number of particles, temperature, and volume were fixed) ensemble MD based on density functional theory (DFT) simulations comprising one oxalic acid and 55 water molecules were performed using the Vienna ab-initio simulations package (VASP) [14,15]. The temperature during this simulation was 300 K, which was controlled using Nose-Hoover [16,17] thermostat. The simulation cell was a cubic cell with a length of 12.1 Å. The oxalic acid in bulk water was set to 1.01 g/cm$^3$, which is in a good agreement with the experimental density (1.02 g/cm$^3$ at 1atm 298.15K) [18]. The simulation was performed until the energy is equilibrated with 0.2 fs time steps. A plane-wave basis set with an energy cutoff of 400 eV was used, and the projector augmented-wave method (PAW) potentials [19,20] was applied to all atoms. The Perdew, Burke, and Ernzerhof (PBE) exchange correlation functional [21,22] was used. The results of DFT-NVT simulation were used as a starting configuration for DFT NVE (number of particles, temperature, and total energy were fixed) ensemble MD simulation. The NVE ensemble

was performed for 4 ps, which time-step was 0.2 fs, and potential was the same as the NVT ensemble.

Next, structure sampling was performed using the result of the NVE ensemble trajectory. A cluster consisting of one oxalic acid molecule and 30 water molecules was sampled. For the cluster obtained by the structure sampling described above, the oxalic acid molecule at the center of these clusters was used to model the $O_{C=O}$,1s and $O_{C-O-}$,1s core-hole state and the core excitation state dynamics simulation, respectively. The time step in this simulation was 0.25 fs and core-hole excitation state dynamics simulations were propagated for 20 fs. These time lengths of MD simulation were sufficiently short for the required spectral resolution for comparison with the experimentally determined decay process. The core-excited oxygen atom was described using the [7s/6p/2d] IGLO-III basis set [23] of Kutzelnigg et al., the remaining oxygens were described [3s/3p/1d] with relativistic effective core potentials basis sets [24]. and TZVP (valence triple-zeta polarization) [25] basis set was employed for all other atoms. The non-core-excitation oxygen atoms were described by effective core potentials. During the 20 fs simulation, the $O_{C=O}$1s and $O_{C=O}$.1s excited-state MD simulations were propagated, and each snapshot was used to calculate the relative line intensities of the XES spectra.

The relative peak intensities from the XES spectra with the core-hole excited state dynamics simulation were calculated within the framework for DFT using the deMon2k code [26]. The PBE exchange correlation functional

was used. The relative peak intensities were evaluated from the dipole matrix element between the core and valence orbitals of different molecules of the cluster.

In order to reproduce the experimental XES spectra, the line spectra obtained from each snapshot of the core hole excitation state dynamics simulation were convoluted with a Gaussian function (FWHM: 0.2 eV). XES spectra obtained from each snapshot were summed up using the weight function (tau: 4.1 fs) [27]. For this structure sampling method, we obtained approximately 20 spectra from the core-hole excited state dynamics of the $O_{C=O}$,1s and $O_{C=O\text{-}}$,1s excitations. The final theoretical XES spectra for each excitation were calculated as the average of these spectra.

### 2-2-2 Liquid ethanol

To construct the structure of ethanol in the liquid phase, classical MD simulations were adopted in the NVT ensemble at 240–340 K and 1 bar using GROMACS 5.1.4 [28] with optimized potentials for liquid simulations (OPLS) force field [29]. Atomic charges were used without further modifications to the implemented code. A simulation box was set up as a cubic box containing 1000 ethanol molecules, and its length was determined to adjust the experimental density for the target temperature. The Verlet integration was applied with an integration time step of 0.2 fs, and a total run of 4 ns for each temperature.

The scheme of calculations of XES profiles followed the previous studies for methanol [30] and ethanol [31]. In the present study, only two extreme cases, such as the lowest and highest temperatures, were adopted, where 17 ethanol clusters were randomly extracted from the final snapshot of the MD simulations. A total of 100 sets of initial structures were sampled at each temperature. We confirmed that the sampling was adequate to describe the XES profiles. XES profiles were computed using the semi-classical Kramers-Heisenberg (SCKH) formula developed by Ljungberg et al. [32]. An O–H bond of the central ethanol molecule in the sampled cluster was geometry-optimized, and by frequency analysis, a positive frequency was obtained, which was assigned to the O–H stretching mode. Multidimensional wavepacket motions were modeled through core-hole state classical MD simulations with the initial conditions, from sampling two positions of

quantum mechanical vibrational probability distribution along with a vibrational mode and four momenta. Each trajectory was propagated for 20 fs in steps of 0.25 fs. This MD run was the minimum to describe the effect of the dynamics on the core-hole state accurately. The oscillator strengths of the transition between the core-hole and final states were calculated for each geometry along the MD trajectory. The final calculated spectra were shifted by 2.8 eV to match the experimental spectra. A core-hole lifetime of 4 fs was applied to the $O_{1s}$ core hole. In the XES calculations, two temperature conditions of 240 and 340 K were applied at lower and higher temperatures. For hydrogen, [2s/2p] basis sets were used. To describe the core-excited oxygen in the central ethanol molecule, the IGLO-III basis sets [23] was used for additional flexibility in the core-region while the remaining oxygens and the carbons were described [3s/3p/1d] with relativistic effective core potentials basis sets [24]. Exchange-correlation functional and DFT code were the same as those used for oxalic acid. To correct entanglement of the potential energy curve and discontinuous of the transition moment, a new scheme with the genetic algorithm developed by Pettersson et al. [33] was applied.

**Network analysis**

The intermolecular local structure around the central molecule was discerned via the number of h-bonding donors or acceptors, that is, D*m*A*n*, where *m* and *n* are the number of h-bonding donors and acceptors,

respectively. Several h-bonding criteria originated from different philosophies such as potential energy, geometry, charge density, or electrostatic potential have been proposed, and their comparison have been performed by Kumar et al.[34], Henchman et al.[35], and Lehtola et al.[36]. In the present study, we used geometrical definition because this definition can be applicable straightforwardly for the results of MD simulations. Lehtola et al.[36] compared the h-bonding behavior of several linear alcohols using three definitions of the h-bonding criteria and observed that the difference in them is primarily the absolute value of the number of h-bonding. In the present study, the definition proposed by Wernet et al. was applied [37], that is, the h-bonding existed if the oxygen–oxygen distance satisfied the following relation,

$$r_{\mathrm{OO}} \leq (3.3 - 0.00044\theta^2) \quad (\text{Å})$$

where, $r_{\mathrm{OO}}$ is the O–O distance, and $\theta$ is the angle (in degree) between the internal OH and O–O directions. Considering the discussion regarding the aforementioned local structure, we analyzed the h-bonding network connectivity by exploiting Johnson's algorithm implemented in the Python language software package NetworkX [38].

### 2-2-3 Liquid water

The calculation method for liquid water is almost the same as that for ethanol described in the previous section, here is briefly described. To construct the structure of water in the liquid phase, classical MD simulations were adopted in the isothermal-isobaric ensemble from 270 to 360 K at intervals of 30 K and 1 bar with a TIP4Pew force field [39]. In a cubic simulation box, 1000 water molecules were included. The Verlet integrator was applied with a time step of 0.2 fs and run for 4 ns for each temperature point. The bond length and water molecule angles were fixed during the above simulations. However, they were relaxed to obtain power spectra, which were obtained by MD simulations in the microcanonical ensemble for 10 ps. Two hundred clusters were sampled at 300 K, and 100 clusters were sampled at temperature range used for sampling and for $D_2O$. Two O-H bonds of the central water molecule in a sampled cluster were geometry-optimized, and six positive vibrational frequencies of three rotations, H-O-H bending, and two O-H stretching modes were used in the analysis. Each trajectory runs 20 fs in steps of 0.25 fs. The spectra were calculated for each geometry along the MD trajectory. The final calculated spectra are shifted by -2.8 eV to match the experimental spectra. The basis sets functionals, exchange-correlation functional, and network analysis are the same as ethanol.

## Reference


[1] H. Ohashi, Y. Senba, H. Kishimoto, T. Miura, E. Ishiguro, T. Takeuchi, M. Oura, K. Shirasawa, T. Tanaka, M. Takeuchi, AIP Conf. Proc. 879 (2007) 523.

[2] Y. Senba, H. Ohashi, H. Kishimoto, T. Miura, S. Goto, S. Shin, T. Shintake, T. Ishikawa, AIP Conf. Proc. 879 (2007) 718.

[3] S. Yamamoto, Y. Senba, T. Tanaka, H. Ohashi, T. Hirono, H. Kimura, M. Fujisawa, J. Miyawaki, A. Harasawa, T. Seike, S. Takahashi, N. Nariyama, T. Matsushita, M. Takeuchi, T. Ohata, Y. Furukawa, K. Takeshita, S. Goto, Y. Harada, S. Shin, H. Kitamura, A. Kakizaki, M. Oshima, I. Matsuda, J. Synchrotron Radiat. 21 (2014) 352.

[4] Y. Harada, M. Kobayashi, H. Niwa, Y. Senba, H. Ohashi, T. Tokushima, Y. Horikawa, S. Shin, M. Oshima, Rev. Sci. Instrum. 83 (2012) 013116.

[5] A. D. Becke, J. Chem. Phys 98 (1993) 5648.

[6] T. Clark, J. Chandrasekhar, G. W. Spitznagel, P. V. R. Schleyer, J Comput. Chem 4 (1983) 294.

[7] P. J. Hay, J. Chem. Phys. 66 (1977) 4377.

[8] A. J. H. Wachters, J. Chem. Phys. 52 (1970) 1033.

[9] K. Raghavachari, G. W. Trucks, J. Chem. Phys. 91 (1989) 1062.

[10] M. Cossi, V. Barone, B. Mennucci, J. Tomasi, Chem. Phys. Lett. 286 (1998) 253.

[11] B. Mennucci, E. Cances, J. Tomasi, J. Phys. Chem. B 101 (1997) 10506.

[12] E. Cances , J. Tomasi, B. Mennucc, J. Chem. Phys 107 (1997) 3032.

[13] M. J. Frisch, G. W. Trucks, H. B. Schlegel, G. E. Scuseria, M.A. Robb, J. R. Cheeseman, G. Scalmani, V. Barone, G. A. Petersson, H. Nakatsuji, X. Li, M. Caricato, A. Marenich, J. Bloino, B. G. Janesko, R. Gomperts, B. Mennucci, H. P. Hratchian, J. V. Ortiz, A. F. Izmaylov, J. L. Sonnenberg, D. Williams-Young, F. Ding, F. Lipparini, F. Egidi, J. Goings, B. Peng, A. Petrone, T. Henderson, D. Ranasinghe, V. G. Zakrzewski, J. Gao, N. Rega, G. Zheng, W. Liang, M. Hada, M. Ehara, K. Toyota, R. Fukuda, J. Hasegawa, M. Ishida, T. Nakajima, Y. Honda, O. Kitao, H. Nakai, T. Vreven, K. Throssell, J. A. Montgomery, Jr., J.E.

Peralta, F. Ogliaro, M. Bearpark, J.J. Heyd, E. Brothers, K.N. Kudin, V.N. Staroverov, T. Keith, R. Kobayashi, J. Normand, K. Raghavachari, A. Rendell, J. C. Burant, S. S. Iyengar, J. Tomasi, M. Cossi, J. M. Millam, M. Klene, C. Adamo, R. Cammi, J.W. Ochterski, R. L. Martin, K. Morokuma, O. Farkas, J. B. Foresman, D. J. Fox, Gaussian 09, Revision A.02. Gaussian, Inc., Wallingford CT.

[14] G. Kresse, J. Furthmüller, Comput. Mater. Sci 6 (1996) 15.

[15] G. Kresse, J. Furthmüller, Phys. Rev. B 54 (1996) 11169.

[16] S. Nosé, J. Chem. Phys. 81 (1984) 511.

[17] W. G. Hoover, Phys. Rev. A 31 (1985) 1695.

[18] Y. Iwasawa, Handbook of Chemistry: Pure Chemistry, 5th ed, 2003.

[19] P. E. Blöchl, Phys. Rev. 50 (1994) 17953.

[20] G. Kresse, D. Joubert, Phys. Rev. B 59 (1999) 1758.

[21] J. P. Perdew, K. Burke, M. Ernzerhof, Phys. Rev. Lett. 78 (1997) 1396.

[22] J. P. Perdew, K. Burke, M. Ernzerhof, Phys. Rev. Lett. 77 (1996) 3865.

[23] W. Kutzelnigg, U. Fleischer, M. Schindler, NMR-Basic Principles and Progress, Springer-Verlag, Heidelberg, 1990.

[24] G. Igel-Mann, H. Stoll, H. Preuss, Mol. Phys. 65 (1988) 1321.

[25] N. Godbout, D.R. Salahub, J. Andzelm, E. Wimmer, Can. J. Chem. 70 (1992) 560.

[26] A. M. Köster, G. Geudtner, A. Alvarez-Ibarra, P. Calaminici, M. E. Casida, J. Carmona-Espindola, V. D. Domínguez-Soria, R. Flores-Moreno, G. U. Gamboa, A. Goursot, T. Heine, A. Ipatov, A. de la Lande, F. Janetzko, J. M. del Campo, D. Mejia-Rodriguez, J.U. Reveles, J. Vasquez-Perez, A. Vela, B. Zúñinga-Gutierrez, D. R. Salahub, deMon2k, The deMon developers, 2018.

[27] R. Sankari, M. Ehara, H. Nakatsuji, Y. Senba, K. Hosokawa, H. Yoshida, A. De Fanis, Y. Tamenori, S. Aksela, K. Ueda, Chem. Phys. Lett. 380 (2003) 647.

[28] M.J. Abraham, T. Murtola, R. Schulz, S. Páll, J. C. Smith, B. Hess, E. Lindahl, SoftwareX 1-2 (2015) 19.

[29] W. L. Jorgensen, J. Tirado-Rives, J. Am. Chem. Soc. 110 (1988) 1657.

[30] M.P. Ljungberg, I. Zhovtobriukh, O. Takahashi, L.G.M. Pettersson, J. Chem. Phys. 146 (2017) 134506.

[31] O. Takahashi, M. P. Ljungberg, L. G. M. Pettersson, J. Phys. Chem. B 121 (2017) 11163.
[32] M. P. Ljungberg, A. Nilsson, L. G. M. Pettersson, Phys. Rev. B 82 (2010) 245115.
[33] L. G. M. Pettersson, O. Takahashi, Theor. Chem. Acc. 140 (2021) 162.
[34] R. Kumar, J. R. Schmidt, J.L. Skinner, J. Chem. Phys. 126 (2007) 204107.
[35] R. H. Henchman, S. J. Irudayam, J. Phys. Chem. B 114 (2010) 16792.
[36] J. Lehtola, M. Hakala, K. Hämäläinen, J. Phys. Chem. B 114 (2010) 6426.
[37] P. Wernet, D. Nordlund, U. Bergmann, M. Cavalleri, M. Odelius, H. Ogasawara, L. A. Naslund, T. K. Hirsch, L. Ojamae, P. Glatzel, L. G. M. Pettersson, A. Nilsson, Science 304 (2004) 995.
[38] A. A. Hagberg, D. A. Schult, P. J. Swart, the 7th Python in Science Conference (SciPy2008), Pasadena, CA, USA, 2008, p. 11
[39] W. H. Hans, C. S. William, W.P. Jed, D. M. Jeffry, J. D. Thomas, L. H. Greg, H. G. Teresa, J. Chem. Phys. 120 (2004) 9665.

# Chapter 3

# Identification of valence electronic states depending on pH in oxalic acid aqueous solution

## 3-1 Introduction

As mentioned in Chapter 1-3, XES can selectively observe the electronic state of solutes in solution to tune the excitation energy. Site selective XES for liquid has been reported insufficiently. Therefore, there is lack of sufficient knowledge of how adaptable the XES for liquid is to complex molecules. In this Chapter, we investigate pH dependence of aqueous oxalic acid, which is more complex than monocarboxylic acid reported in the several literatures [1-7], using theoretical and experimental analysis.

### 3-2 The conformation stability in oxalic acid aqueous solution

Table 3-1 shows a summary of the calculated energies of several coordinated conformers of oxalic acid in the neutral, anionic, and dianionic forms. In the neutral form, cTc is the most stable conformer in the gas phase. According to PCM and DFT calculations, however, in aqueous solution, tCt is the most stable. This result is in agreement with previous studies [8,9]. For the anionic form, the most stable conformer based on DFT calculations is $tC^-$. The most stable structure calculated by DFT is different between the most stable structure of PCM and the model in the gas phase. Since water molecules around oxalic acid are treated explicitly in terms of the first principles NVT DFT simulations, it is expected that the result of NVT DFT is more reliable than that of the PCM in this case. These results are consistent with the previous studies using the BLYP/def2-SVP theory, where the free energy of $tC^-$ containing 32 water molecules was more stable than the free energy of $cT^-$ [10]. Therefore, $tC^-$ was chosen as the starting configuration for the NVE-ensemble DFT-MD simulation of the anionic form. In the case of the dianionic form, the most stable conformer is dianion-open, which has a twisted dihedral angle (90°). This result is in agreement with previous studies [10-12]. According to the above results, tCt, $tC^-$, and dianion-open were chosen as the starting configurations of the neutral, anionic, and dianionic forms, respectively.

Table 3-1: Energies (units in kJ $mol^{-1}$) are in Gas model, PCM model and DFT NVT model of oxalic acid. Gas and PCM method is calculated by B3LYP/6-311++G(d,p) level of theory. Energies are in kJ/mol.

| Neutral | cTc | tCt | tTt | cTt |
|---|---|---|---|---|
| Gas[a] | 0.00 | 15.14 | 5.77 | 7.53 |
| PCM[b] | 0.78 | 0.00 | 1.71 | 1.92 |
| DFT NVT[c] | 75 | 0 | 83 | 763 |
| Anion | $cT^-$ | $tC^-$ | | |
| Gas[a] | 0.00 | 48.82 | | |
| PCM[b] | 0.00 | 23.07 | | |
| DFT NVT[c] | 36 | 0 | | |
| Dianion | Open | Close | | |
| Gas[a] | 0.00 | 0.02 | | |
| PCM[b] | 0.00 | 0.00 | | |
| DFT NVT[c] | 0 | 6 | | |

(a) Single oxalic acid in the gas phase.

(b) Single oxalic acid with PCM method.

(c) Single oxalic acid in 30 water molecules.

### 3-3 Structure of aqueous oxalic acid

The dihedral angles between the two carboxyl groups of the aqueous oxalic acid conformers are shown in Table 3-2. The dihedral angles of the neutral and anionic forms are close to 0°, and their deviations are small compared to that of the dianionic form. Thus, two carboxyl groups in the neutral and anionic forms are parallel and scarcely twisted. In contrast, that of the dianionic form is close to 90°, with a large deviation. This shows that the two carboxyl groups in the dianionic form of aqueous oxalic acid have a perpendicular configuration that is more rotatable compared to the neutral and anionic forms. This feature, which is discussed in a later section, plays an important role in differentiating it from acetic acid.

Table 3-2: Average and deviation of dihedral angle (units in degree) between two carboxyl groups of aqueous oxalic acid in neutral, anionic and dianionic form by the DFT NVT method. Optimized dihedral angles by the PCM are also shown.

| | Neutral | Anionic | dianionic |
|---|---|---|---|
| Average (standard deviation) | 18 (8) | 10 (10) | 67 (12) |
| PCM | 0.002 | 10.004 | 89.002 |

### 3-4 Comparison with the experimental and theoretical spectra

The experimental and theoretical XAS spectra around the first resonant peaks of aqueous oxalic acid at the O K-edge are shown in Figures 3-1a and b. The insets show the wider energy range of 530–550 eV. Clear peak structures are observed at ≈ 531.7 (pH 1.1), 532.0 (pH 2.7), and 532.4 eV (pH 12.9). According to the previous report of acetic acid [4], the peak structure at ≈ 532 eV, which is not due to water absorption, can be assigned to $O_{C=O}$1s and $O_{C\text{-}O^-}$ 1s to π* transitions of carboxyl groups in the solvent (water). The energy region larger than 534 eV contains the O *K*-edge absorptions of oxalic acid and water.

The experimental results exhibit energy shifts and changes in peak intensity. In the π* peak region (≈ 532 eV), the theoretical XAS spectra well reproduce these trends. In the region larger than 534 eV, the reproducibility of the theoretical spectra is poor. While the theoretical spectra contain only 30 molecules of water absorption, the experimental spectra reflect contributions from a large amount of water absorption, in principle. Therefore, the number of water molecules used in the calculations were enough to simulate in solution.

The pKa values of oxalic acid are 1.25 and 3.81 [13]. According to the Henderson-Hasselbalch equation, the oxalic acid conformers at pH 1.1, 2.7, and 12.9 are almost purely neutral, anionic, and dianionic forms, respectively. Thus, the experimental spectra at pH 1.1, 2.7, and 12.9 were compared to the theoretical spectra of the neutral, anionic, and dianionic conformers,

respectively.

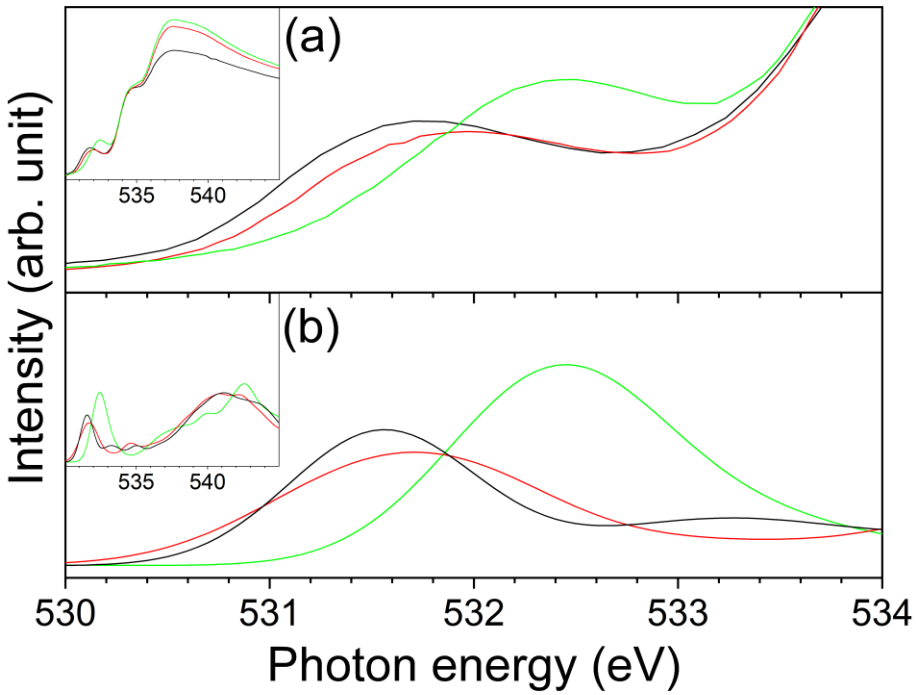


Figure 3-1: (a) Experimental and (b) theoretical XAS spectra of oxalic acid (black: pH 1.1, red: pH 2.7, green: pH12.9).

The experimental and theoretical XES spectra of aqueous oxalic acid at the O K-edge are shown in Figures 3-2a and 3-2b. The theoretical XES spectra were obtained through summation, using ratios estimated from the intensities of the theoretical XAS spectra. The energy and intensity of each theoretical spectrum was shifted -0.85 eV and normalized to fit the experimental first resonant peak of pH 12.9. In the experimental spectra, the intensity of the highest energy peak position (first peak, ≈ 526.5 eV) at pH 2.7 is lower than that at pH 1.1. The energy of first peak at pH 12.9 red-shifts and the intensity is higher than that at pH 1.1 and 2.7. For the peak at ≈ 525 eV (second peak), the intensity at pH 12.9 is higher than that at pH 1.1 and 2.7. Regarding the peak energy, the second peak blue-shifts as the pH value increases. Regarding the trend of the energy shift due to pH variation, the theoretical XES spectra well reproduce the experimental XES spectra. Note that the absolute values of the theoretical emission energies do not well coincide with those of the experimental values because the theoretical energy values were obtained from orbital energy differences which did not account for relaxation effects.

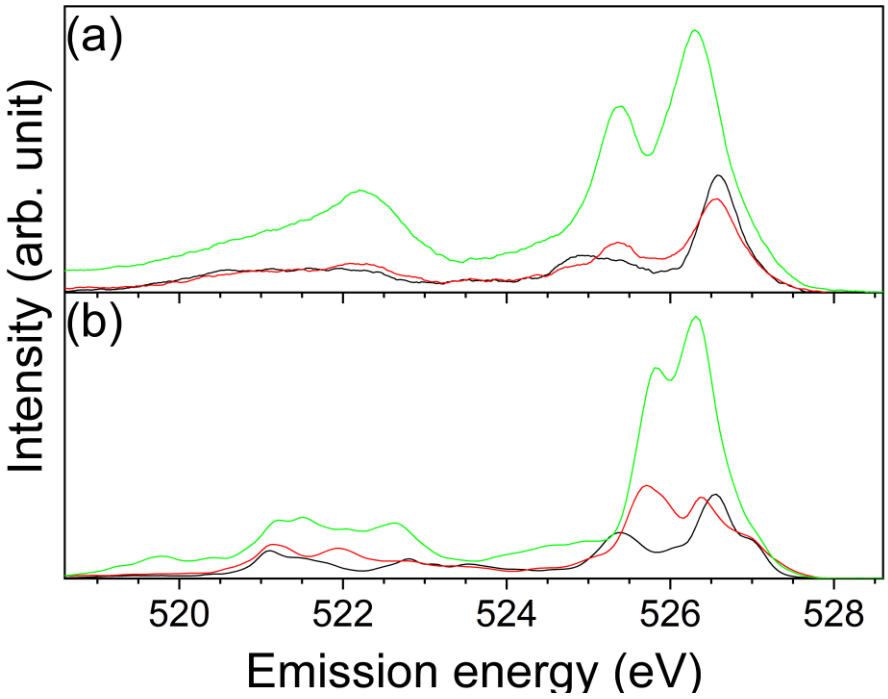

Figure 3-2: (a) Experimental and (b) theoretical XES spectra of oxalic acid (black: pH 1.1, red: pH 2.7, green: pH12.9).

### 3-5 Assignment of soft x-ray spectra

Figures 3-3 to 3-5 show detailed assignments of MOs for the XES spectra using cluster models of: Figure 3-3 neutral, 3-4 anionic, and 3-5 dianionic conformers. Theoretical absorption spectra for each form are also shown as insets. In order to discuss the assignment of each peak, line spectra with corresponding MOs obtained from single-molecule models are also shown.

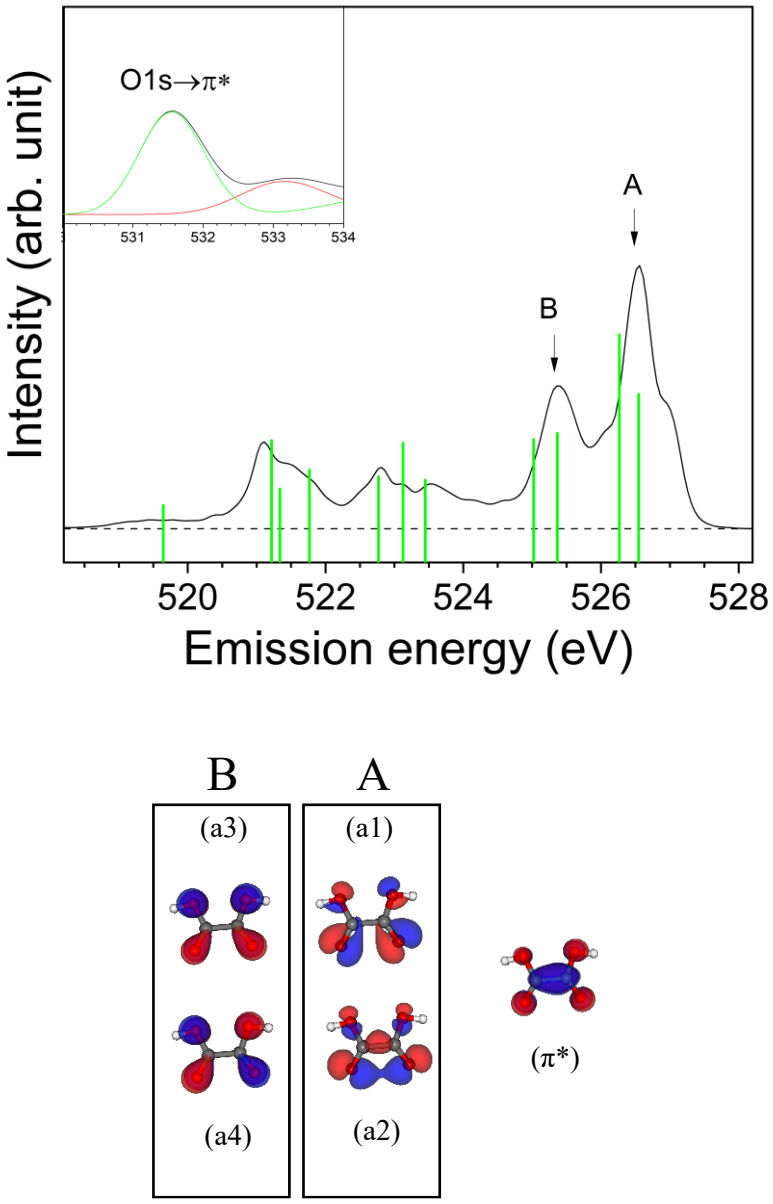


Figure 3-3: O1s XES and XAS (inset) of neutral oxalic acid and corresponding orbital to each peak. The black line is the sum of spectra of all oxygen atom which expected to contribute to the spectra (red: OH green: CO). Line spectra are obtained from single molecules models.

In the neutral form (Figure 3-3), only the $O_{C=O}$ 1s excitation contributes to the first resonance peak in the XAS spectrum. Therefore, the XES spectrum of the $O_{C=O}$ 1s excited state is shown. The spectrum from the cluster model corresponds well to the spectrum from the single molecule model. Comparison of the theoretical XES spectra using the single molecule model and the cluster model shows that MO a1 and a2 associated with the in-plane respect to the carboxylic group correspond to peak A. MOs a3 and a4 associated with the out-of-plane respect to the carboxylic group correspond to peak B. Comparing the theoretical and experimental spectra, it is shown that peaks A and B correspond to the first and second peaks, respectively.

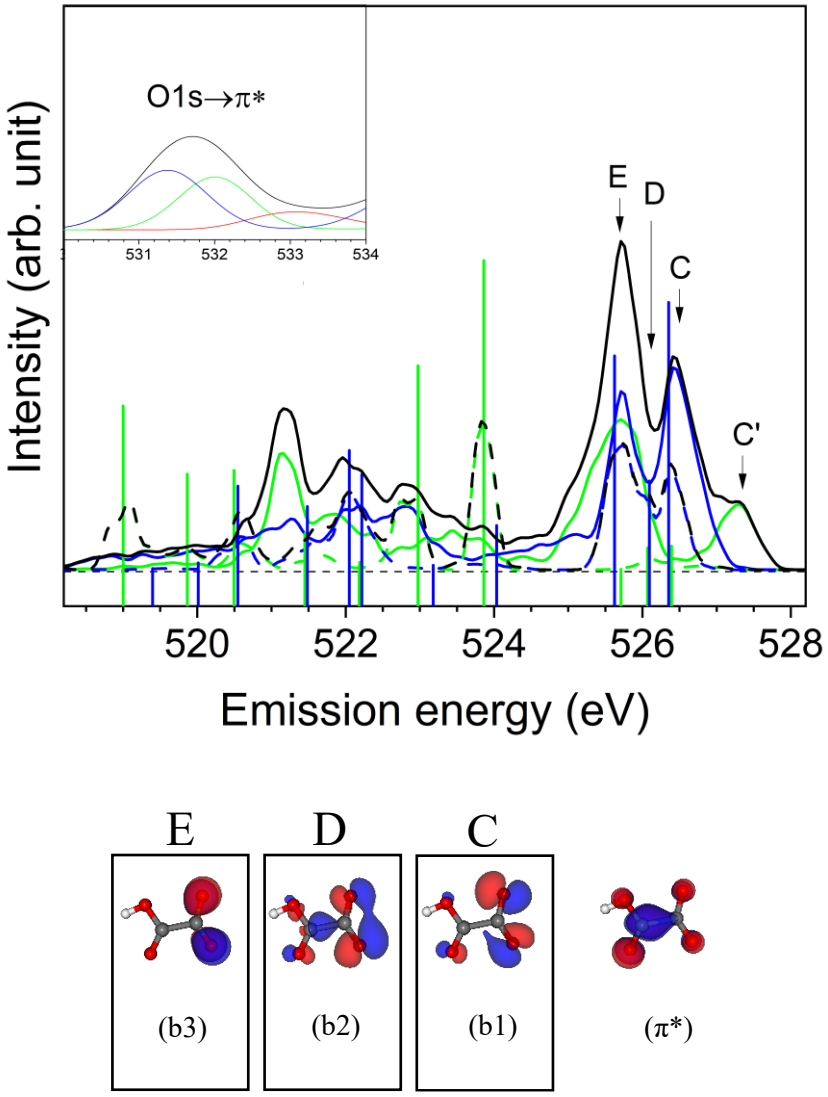


Figure 3-4: O1s XES and XAS (inset) of anionic oxalic acid (black line: the sum of all spectra, red: OH green: CO, O blue: $CO^{-}$, line: single molecule)

In the anionic form (Figure 3-4), the $O_{C=O}$ 1s and $O_{C-O^-}$ 1s excitation peaks contribute to the first resonance peak in the XAS spectrum. Therefore, the emission spectra were calculated taking into account both the $O_{C=O}$ 1s and $O_{C-O^-}$ 1s excited states. By comparing the single molecule model with the theoretical emission spectra using the cluster model, MOs b1 and b2 associated with the in-plane show peaks C and D, respectively. MO b3, associated with the out-of-plane, shows peak E. In the case of $O_{C-O^-}$, the spectra from the cluster model correspond well to those of the single molecule model. On the other hand, the spectrum of the cluster model for $O_{C=O}$ differs from the spectrum of the single molecule model. Peak C' does not exist in the single molecule model, but appears only in the cluster model with $O_{C=O^-}$ Therefore, we can assume that peak C' is the result of the interaction between oxalic acid and solvent (water). Comparing the theoretical spectrum with the experimental spectrum, peaks C, C', and D correspond to the first peak, and peak E corresponds to the second peak.

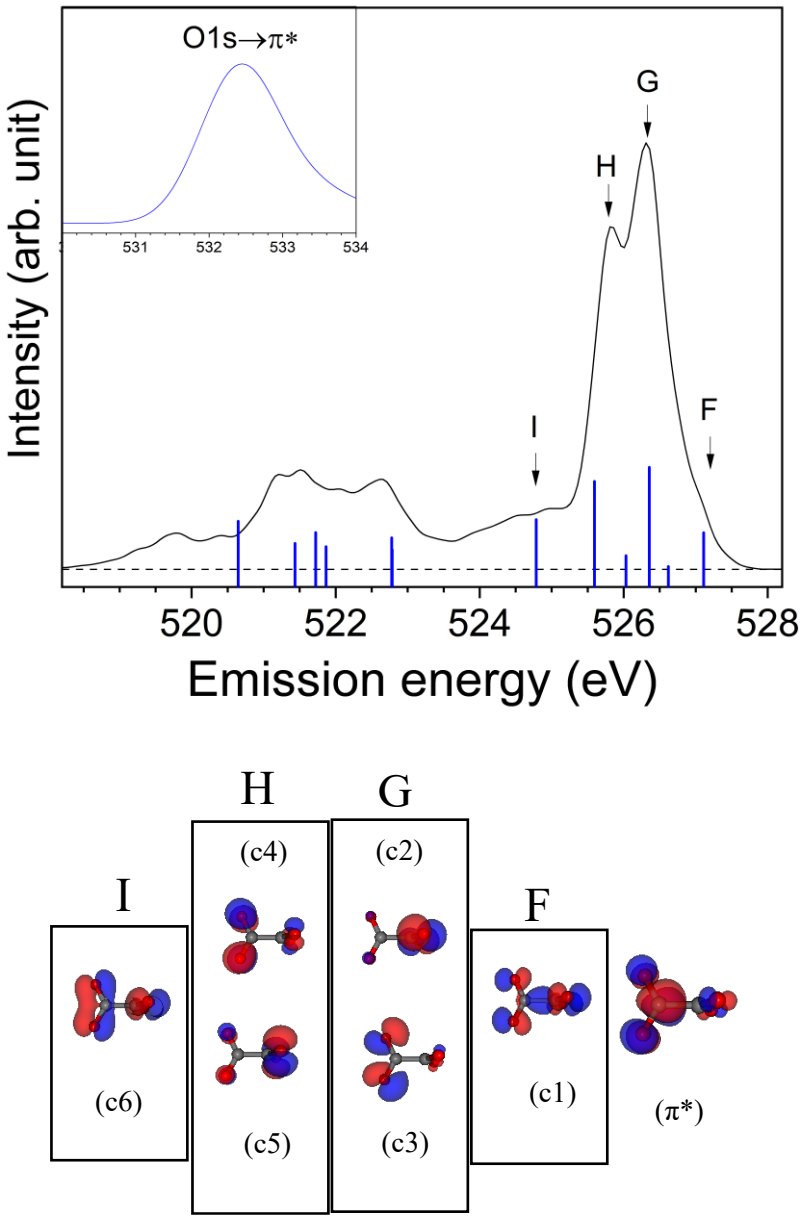


Figure 3-5: O1s XES and XAS (inset) of dianionic oxalic acid (black line: the sum of all spectra, O blue: $CO^{-}$, line: single molecule)

In dianionic form (Figure 3-5), only the $O_{C\text{-}O}^{-}$ 1s excitation peak contributes to the first resonant peak in the absorption spectrum. Therefore, the emission spectrum was calculated solely for the $O_{C\text{-}O}^{-}$ 1s excited state. MOs c1, c2 and c3, and c6, associated with in-plane, exhibit peaks F, G, and I, respectively. Out-of-plane MOs c4 and c5 exhibit peak H. Comparing the theoretical and experimental spectra, peaks F and G correspond to the first peak, and peak H corresponds second peak.

### 3-6 Comparison with acetic acid

In the experimental XAS spectra, the first peak at 532 eV assigned as $O_{C=O}1s$ to π* excitation blue-shifts with increasing pH (approximately ≈ 0.7 eV). For monocarboxylic acids, similar blue-shifts of the first absorption peak caused by deprotonation were reported [4,7]. Therefore, interestingly, the blue-shift between pH 1.1 and 12.9 for oxalic acid is approximately two times larger than that observed for acetic acid. The difference in the blue-shifts between acetic and oxalic acids can be explained by delocalization of the MOs. This delocalization is caused by resonance of two π* MOs of carboxyl groups. The π resonance is sensitive to the dihedral angle of the COO planes of the two carboxyl groups. According to the single-molecule model calculations, for pH 1.1 and 2.7, the dihedral angles are 15 and 10.8°, respectively. In contract, the dihedral angle dramatically changes at pH 12.9, becoming 69.5°. This large dihedral angle generates two parallel carboxyl groups in a twisted configuration, which breaks π resonance and making the first resonant absorption peak further blue-shifted.

In the experimental XES spectra, the first peaks (A, C, and G), which consist of in-plane MOs (a1, a2, b1, c2, and c3) red-shifts with increasing pH. The second peaks (B, E, and H), which consist of out-of-plane MOs (a3, a4, b3, c4, and c5), blue-shift with increasing pH. The blue-shifts of the second peaks almost cease when deprotonation of one side of the carboxyl group is complete. These trends in energy shifts are similar to those observed by XES of monocarboxylic acids. According to the previous study of acetic

acid [4], the shifts of the first and second peaks can be explained by deprotonation of the carboxyl group. The MOs in the first and second peaks of the anionic and dianionic forms are localized to one side of the carboxyl group. Therefore, these MOs are considered to be almost independent of the other carboxyl groups. Therefore, the shift observed for oxalic acid can also be explained by deprotonation of the carboxyl group.

## 3-7 Conclusion

XAS and site selective XES were used to study the change in the electronic structure of oxalic acid in bulk water with pH. These experimental results were combined with spectral simulation XAS and XES data using DFT calculations and ab initio MD simulations of the liquid structure model. The experimental XAS and XES results showed a pH-dependent change in the spectra. The theoretical spectra reproduce well the pH-dependent changes in the experimental spectra, demonstrating the importance of including solvent effects. By combining theoretical and experimental analysis, the electronic state of oxalic acid in aqueous solution was clarified. The pH-dependent changes in the spectra were found to reflect not only the ionization of the carboxyl groups, but also the angular twist between these groups. In particular, the large difference in the spectra between the anionic and dianionic forms, which was not observed for the monocarboxylic acids, indicates the significant influence of resonance effects between the two carboxyl groups.

## Reference


[1] Y. Horikawa, T. Tokushima, O. Takahashi, Y. Harada, A. Hiraya, S. Shin, Phys. Chem. Chem. Phys. 20 (2018) 23214.

[2] Y. Horikawa, T. Tokushima, Y. Harada, O. Takahashi, A. Chainani, Y. Senba, H. Ohashi, A. Hiraya, S. Shin, Phys. Chem. Chem. Phys. 11 (2009) 8676.

[3] Y. Horikawa, T. Tokushima, A. Hiraya, S. Shin, Phys Chem Chem Phys 12 (2010) 9165.

[4] T. Tokushima, Y. Horikawa, Y. Harada, O. Takahashi, A. Hiraya, S. Shin, Phys. Chem. Chem. Phys. 11 (2009) 1679.

[5] N. Nishida, T. Tokushima, O. Takahashi, Chem. Phys. Lett. 649 (2016) 156.

[6] N. Nishida, S. Kanai, T. Tokushima, Y. Horikawa, O. Takahashi, Chemical Physics Letters 640 (2015) 55.

[7] B. M. Messer, C. D. Cappa, J. D. Smith, K. R. Wilson, M. K. Gilles, R. C. Cohen, R. J. Saykally, The Journal of Physical Chemistry B 109 (2005) 5375.

[8] G. Buemi, J. Phys. Org. Chem. 22 (2009) 933.

[9] K. H. Weber, F.J. Morales, F. M. Tao, J Phys. Chem. A 116 (2012) 11601.

[10] O. Kroutil, B. Minofar, M. Kabelac, J. Mol. Model. 22 (2016) 210.

[11] H. J. Maria, S. P. McGlynn, J. Mol. Spectrosc. 42 (1972) 177.

[12] D. G. Kuroda, R. M. Hochstrasser, Phys. Chem. Chem. Phys. 14 (2012) 6219.

[13] D. R. Lide, CRC handbook of chemistry and physics, 2005.

# Chapter 4

# Soft X-ray emission spectroscopy of liquid ethanol reflecting the change of h-bonding depended on temperature

## 4-1 Introduction

In XES for liquid, it is known that hydrogen bonding has a significant effect on the spectra, while its interpretation is controversial. Ethanol is the simple molecule with a structure contains only one OH bond, for h-bonding structure. As mentioned in Chapter 1-5, several studies about the local structure of liquid ethanol are reported [1-12], and these studies claim that h-bonding plays an important role in the local structure of liquid ethanol. However, direct observation of the hydrogen bonding structure of liquid ethanol has not been studied.

In this Chapter, XES of liquid ethanol are compared experimentally and theoretically in the local structure changes, using temperature as a parameter to changes the interactions in the system. Based on the changes in hydrogen bonds obtained by local structure analysis, we investigated how they affect the XES spectra.

## 4-2 Experimental results

To identify changes in the h-bonding structure of liquid ethanol with increasing temperature, XES measurements were performed using temperature-controlled liquid cells at 241 and 313 K. The intensity at (1) 526.5 eV decreased, and the intensity at (2) 527.5 eV slightly increased with increasing temperature, shown in Figure 4-1. In the previous study [12], the intensity of the peak at the 527.5 eV is enhanced as the oxygen–oxygen distance and OH–O angle increase.

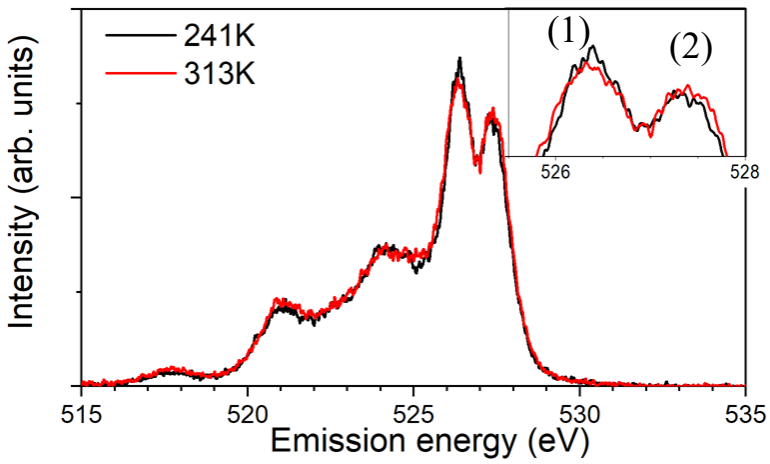


Figure 4-1: Experimental temperature dependence of O 1s non-resonant XES spectra of liquid ethanol (inset is in the range of 526.5 eV to 528 eV). The XES spectra of liquid ethanol at different temperatures normalized to the area intensity.

## 4-3. Theoretical results

### 4-3-1 Theoretical XES spectra

Figure 4-2 shows the calculated XES profiles of ethanol depending on temperature. The spectral characteristics of ethanol at 240 and 340 K below 525 eV are similar, and significant differences in the spectra are observed in the two peaks at (1) 526.5 eV and (2) 527.5 eV. In the previous report [12], the two peaks at 526.5 eV and 527.5 eV are assigned as in-plane and out-of-plane lone pairs against an O–C–C plane. The assignment of these two peaks will be discussed again in a later section. The intensity of the peak at 526.5 eV decreases with increasing temperature, however, that of the peak at 527.5 eV increases, which is consistent with experimental results. The difference between the calculated and experimental spectra may be due to the temperature range and the theoretical modeling. The temperature range of the theory was 240-340 K, but the temperature range of the experiment was 241-313 K. The temperature effect from the theory is improved over the experiment. Several limitations are applied to theoretical modeling; for example, sampling of the vibration is sampled only for the OH stretching vibration defined by the initial structure. The ethanol has the 21 vibrational modes. In this study, only the OH stretching vibrations were sampled because they have been reported to be the most influential on the XES spectra of hydrogen-bonded structures [13-15]. This limitation accentuates the effect of OH stretching motion on the spectrum. Other factors, for example, the selection of basis sets, force fields, and exchange-correlation functionals,

may also enhance the difference between experiments and calculations.

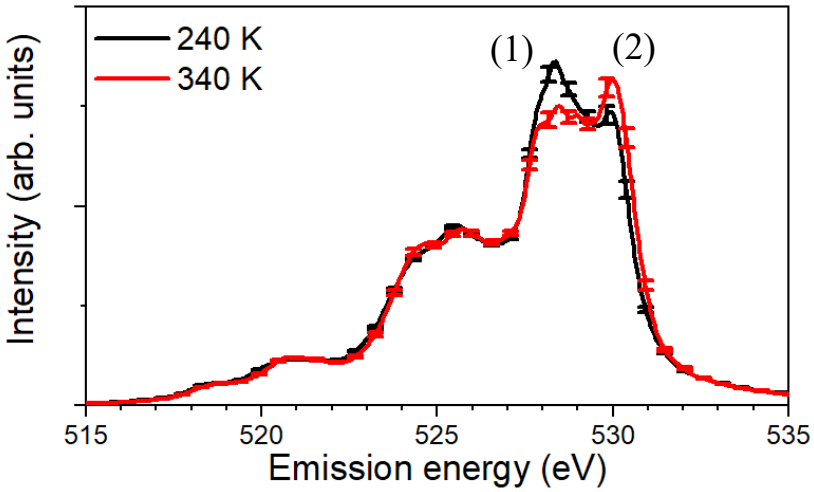


Figure 4-2: Comparison of the calculated XES spectra at 240K (black) and 340K (red). The error bars represent the standard error.

### 4-3-2 The oxygen-oxygen pair radial distribution function

Figure 4-3 shows the oxygen–oxygen RDF of liquid ethanol as a function of temperature in the range of 240–340 K in 20 K steps. The position of the first peak is in good agreement with the experimental value of 2.8 Å observed at 298 K [8]. The first peak broadened and decreased in intensity as the temperature increased. The number of neighboring oxygen atoms in the first peak is approximately two at all temperatures.

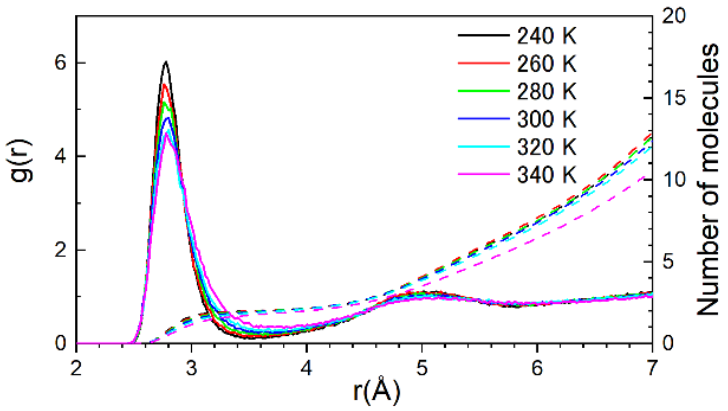


Figure 4-3: The oxygen-oxygen pair radial distribution function (RDF) of liquid ethanol at 240 K (black), 260 K (red), 280 K (green), 300 K (blue), 320 K (light blue) and 340 K (purple) as solid lines. The number of molecules is shown as dashed lines.

### 4-3-3 The analysis of local h-bonding statistics

The histogram of local h-bonding statistics depending on the temperature is shown in Figure 4-4b. “Sum” is defined by the sum of all types of h-bonds. As the temperature increases, the ratios of D1A1, D1A2, and the sum of all types of h-bonding decrease. On the other hand, the ratios of D0A0, D1A0, and D0A1 increase. Figure 4-4c shows the comparison of several h-bonding definitions [16,17]. For all definitions, the trend of local h-bonding statistics depending on the temperature was consistent. To elucidate breaking h-bonding, the increase in the kinetic energy of the molecule is taken into account. This contributes to the breaking of h-bonds. The type of h-bond that shows significant variation is D1A1, indicating that the decay of D1A1 with increasing temperature is a key event in the breaking of h-bonds. According to the RDF shown in Figure 4-3, the number of oxygen atoms in the first shell is about two, even with increasing temperature. Thus, the orientation of hydrogen is disturbed. In other words, the local breaking of h-bonding structure occurs; in contrast, the distance between the oxygen atoms in O–O pair remains intact.

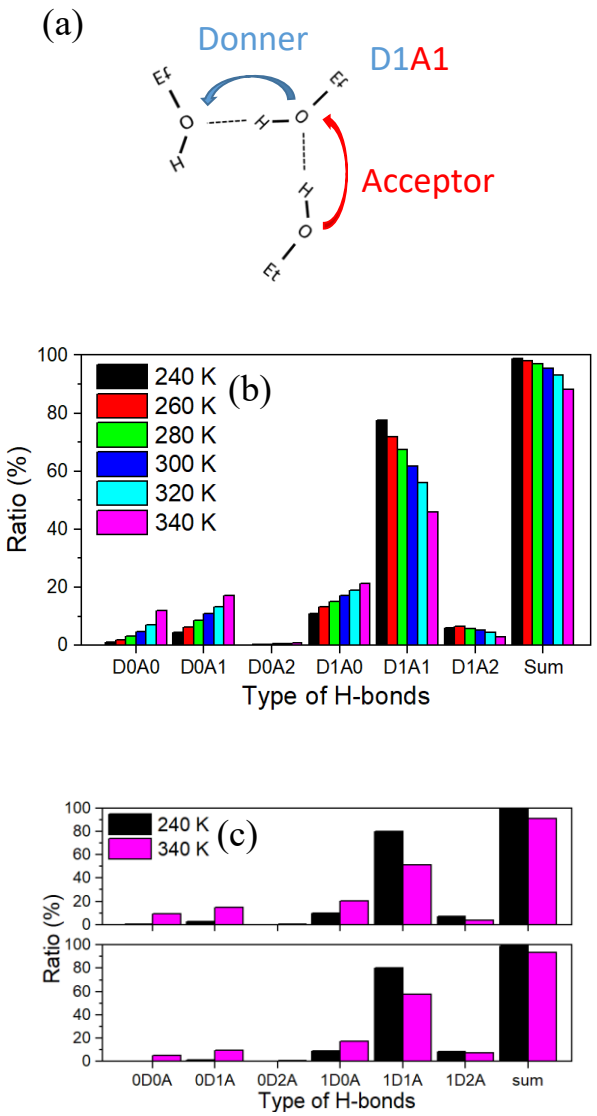


Figure 4-4: (a) The D1A1 of ethanol clusters are illustrated.
(b) The histogram of local h-bonding statistics depending on temperature. D*m*A*n* represents that the number of H-bond donors and acceptors are *m* and *n*, respectively. "Sum" is the sum of all types of h-bonds except for isolated molecule.
(c) The histogram of local h-bonding statistics depending on temperature for three h-bonding definitions. Top defined by Haughney et. al. [16], bottom defined by Chen et.al. [17].

### 4-3-4 The analysis of large cluster structure

The structure of liquid ethanol clusters was further identified by correlating them with the local h-bonding connectivity. Figure 4-5 shows the population of the three structural types of ethanol clusters at each temperature. The linear type of the cluster has D0A1 and D1A0, which are connected by a chain of several D1A1s, shown in Figure 4-5a. In a branched type structure, one or more branches of D1A2 exist in the linear type structure. The ring type structure contains cyclic chain ethanol. Figure 4-5b shows the number of clusters in each structure. As the temperature increases, the sum of all cluster types and the number of linear types increases significantly. However, the branch and ring types remain stable. Therefore, the cluster types obtained by increasing the temperature appear to be linear. Figure 4-5c shows a histogram of the cluster size; the maximum size of clusters in the range of 240–340 K at each 20 K step is 321, 264, 188, 112, 74, and 41, respectively, that is, decreasing monotonically. With an increase in temperature, the number of small clusters of less than five molecules increased. These results were consistent with the simulations from previous studies [4,8,18]. Considering the analysis of h-bonding, these results indicate the breaking process of the h-bonding network with increasing temperature. Large branch clusters were formed in the ethanol solution at 240 K. The D1A1 h-bonding of large branch clusters breaks, and small linear clusters are produced with an increase in temperature.

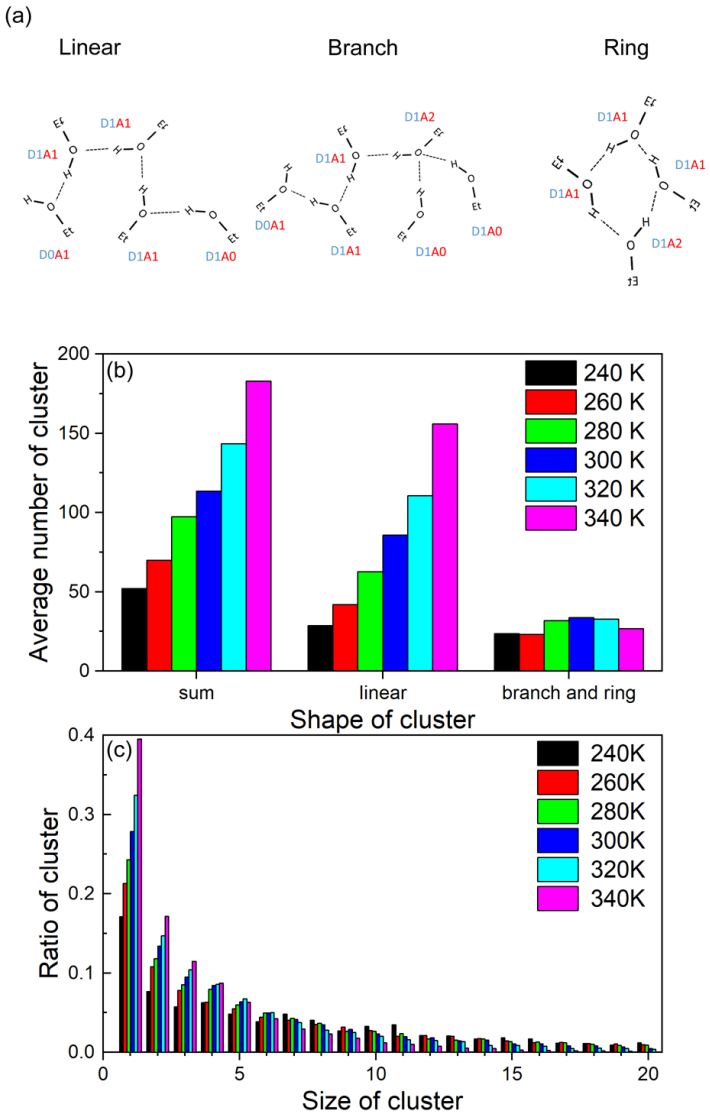


Figure 4-5: (a)The three structural types of ethanol clusters are illustrated. (b)The number of clusters in each structure and (c) the histogram of the size of the cluster. The maximum size of clusters from 240 to 340 K in 20 K steps are 321, 264, 188, 112, 74, and 41, respectively.

### 4-3-5 Effect of local h-bonding on XES spectra

In order to identify the effect of local h-bonding configurations on the XES profile, the simulated liquid ethanol spectrum was decomposed into several h-bonding types. Figure 4-6 shows the spectra of the local structures of D0A1, D1A0, and D1A1, the major h-bonding configurations contributing to the ethanol cluster, with each spectrum normalized independently. The peak at (1) 526.5 eV for D1A1 and D1A0 is larger than the peak at (2) 527.1 eV at both temperatures. In contrast, the peaks for D0A1 were comparable. These results indicate that the $I_{527.5/I526.5}$ intensity ratio of the peaks depends on the type of h-bonding configuration. According to the histogram of local h-bonding statistics, shown in Figure 4-4, and the spectra of the local structure, shown in Figure 4-6, the change in the spectra with temperature corresponds to the change in the ratio of intensities of the h-bonding type.

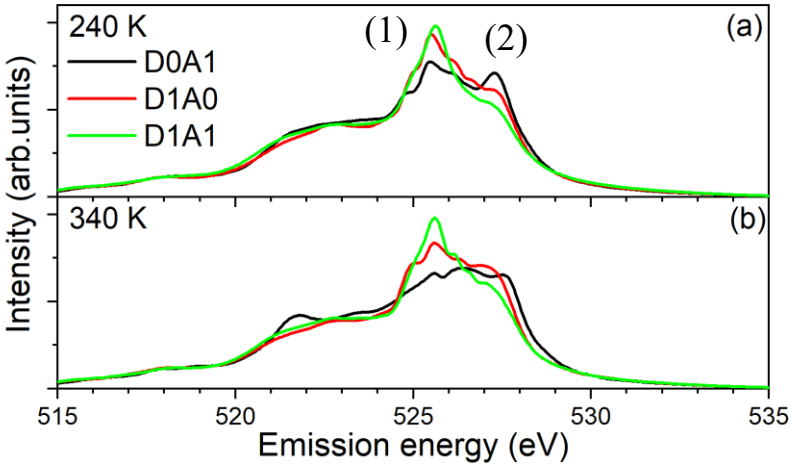


Figure 4-6: The XES spectra in 240 K (up) and 340 K (bottom) for D0A1 (black), D1A0(red), and D1A1 (green).

### 4-3-6 Attribution of XES spectra

In order to understand the effect of local h-bonding configurations on the valence electrons, the XES spectra were decomposed into valence orbitals. As shown in Figure 4-7, at 240 and 340 K, the spectra were decomposed into orbital contributions, with the highest orbitals of the 17 ethanol molecules assigned to 3a", the next 17 to 10a', and so on. Each orbital is identified based on the energy order of a single molecule. At both temperatures, the component assigned as 3a" shows split peaks at (1) 526.5 eV and (2) 527.5 eV, and the ratio of their intensities ($I_{527.5/I526.5}$) increases with temperature. In contrast, the component assigned to the other orbitals shows one broad peak. In the previous study [12], the peaks at 526.5 and 527.1 eV were assigned as 10a' and 3a", respectively. However, to compare with Figure 4-2, a mixed state of 3a" and 10a' is assigned to the peak at 526.5. The interpretation of the peaks at 526.5 and 527.1 eV is rationalized by the following detailed analysis.

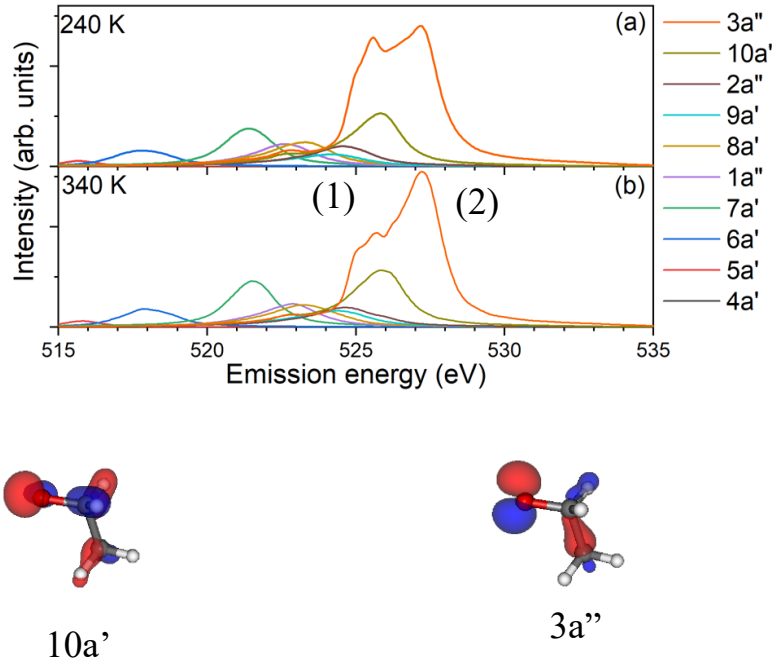


Figure 4-7: The component from each orbital of the XES spectra in 240 K (up) and 340 K(bottom).

Figure 4-8 shows the contribution of each orbital component to the calculated XES profiles separated for different h-bonding configurations. At both temperatures, the spectra assigned as 3a" (orange) for D1A1 and D1A0 show double peaks at (1) 526.5 and (2) 527.5 eV, while the spectra assigned as 3a" for D0A1 show a single peak at (2) 527.5 eV with a small shoulder at (1) 526.5 eV.

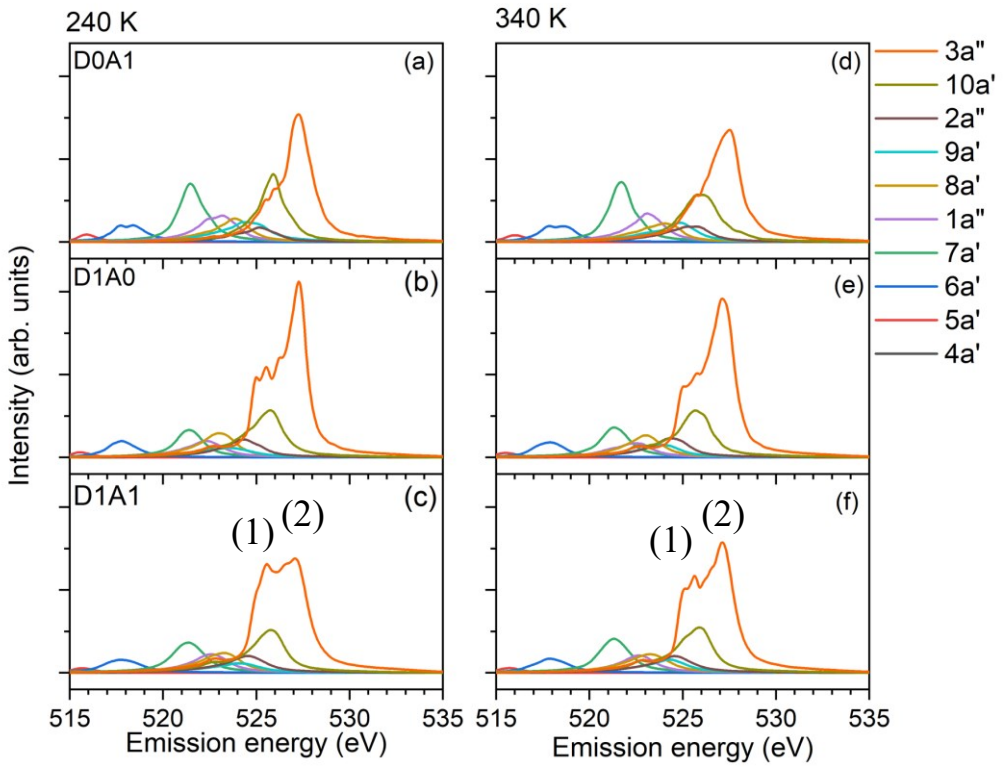


Figure 4-8: Contribution of each orbital component to the XES spectra in 240 K (left) and 340 K (right) for D0A1 (a, d), D1A0 (b,e) and D1A1 (c,f). The component from each orbital of the XES spectra in 240 K (left) and 340 K(right) for D0A1 (a, d), D1A0 (b,e) and D1A1 (c,f) configurations.

### 4-3-7 Effect of local hydrogen bonding on dynamics

To identify the cause of the peak splitting of the 3a” component, Figure 4-9 shows time propagations within 10 fs of the theoretical XES profiles. In all the spectra at 0 fs, corresponding to the moment of electronic excitation, the intensities at (1) 526.5 eV, which corresponds to the second-highest energy peak, are weaker than those at (2) 527.5 eV, which is corresponds to the highest energy peak. In both temperatures, the intensities of peaks at approximately 526.5 eV for D1A1 and D1A0 increase substantially, and that of the peaks at approximately 527.5 eV decrease, as time progresses. In contrast, for D0A1, the intensities changes at approximately 526.5 and 527.5 eV are small. Therefore, the cause of the splitting of the 3a" component for D1A1 and D1A0 is the increase in the intensities at approximately 526.5 eV, caused by the core-hole-induced dynamics. The h-bonding configuration plays an important role in understanding the temperature dependence of the XES profiles.

The effect of nuclear dynamics in liquid alcohol was discussed by Ljungberg et. al. [13]. The XES study of methanol at 300 K was performed theoretically, and the spectrum showed a double peak at 526 eV and 527 eV. This corresponds to peaks at 526.5 and 527.5 eV of ethanol. Deuterium-substituted methanol ($CH_3OD$) has a higher peak intensity at 527 eV than that of methanol ($CH_3OH$). This difference in the spectra is caused by the "dynamical effects" due to the deuterium substitution. In the present study, the intensity of the peak at 527.5 eV increases with increasing temperature.

The difference in the spectrum is caused by "dynamical effects" due to “h-bonding structures changing” depending on temperature.

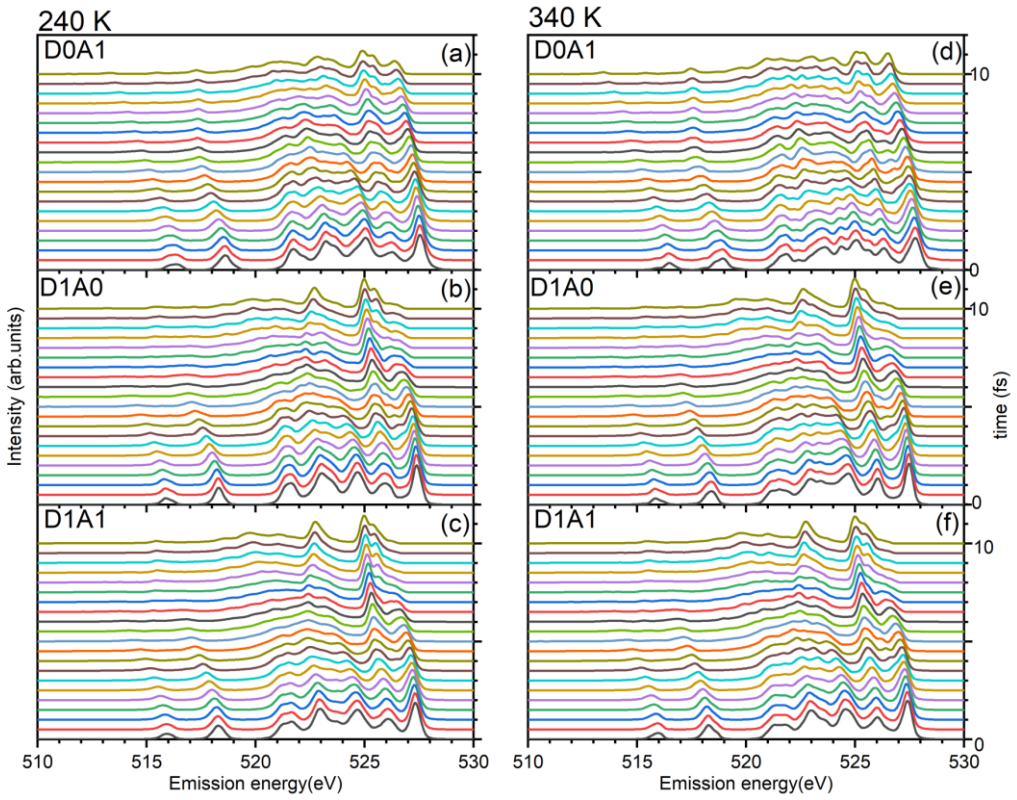


Figure 4-9: The time propagations within 10 fs of the theoretical spectra component for D0A1 (a,d), D1A0 (b,e) and D1A1 (c,f).

### 4-3-8 Conclusion

The temperature dependence of the valence electronic structure of liquid ethanol has been investigated using experimental and theoretical XES profiles. The main change in the XES profiles is the intensity change of the peaks at 526.5 and 527.5 eV with increasing temperature. The peaks at 526.5 and 527.5 eV, which were assigned as 3a" and 10a', respectively, in previous studies, have been modified: the peak at 526.5 eV is a mixture of the 3a" and 10a' components, while the peak at 527.5 eV constitutes 3a". The splitting of the 3a" component occurred due to the h-bonding behavior of liquid ethanol. Theoretical analysis showed that as the temperature increases, the kinetic energy of the ethanol molecule increases and h-bonds are broken, resulting in a decrease in the number of D1A1. When h-bonds are cleaved at high temperatures, the large branching structures that are primarily responsible for the low temperatures are replaced by smaller linear structures. The change in intensity of the XES profile with increasing temperature is caused by a decrease in D1A1. These results suggest that the electronic structure of liquid ethanol reflects several types of h-bonded structures and that the ratio of these h-bonded types changes with temperature.

## References


[1] A. Turanov, A. K. Khitrin, Ind. Eng. Chem. Res. 55 (2016) 9952.

[2] R. Ghanghas, A. Jindal, S. Vasudevan, J. Phys. Chem. B 124 (2020) 662.

[3] P. G. Jönsson, Acta Cryst. B 32 (1976) 232.

[4] A. Vrhovsek, O. Gereben, A. Jamnik, L. Pusztai, J. Phys. Chem. B 115 (2011) 13473.

[5] A.H. Narten, A. Habenschuss, J. Chem. Phys. 80 (1984) 3387.

[6] I. A. Finneran, P. B. Carroll, M. A. Allodi, G. A. Blake, Phys. Chem. Chem. Phys. 17 (2015) 24210.

[7] T. A. Dolenko, S. A. Burikov, S. A. Dolenko, A. O. Efitorov, I. V. Plastinin, V. I. Yuzhakov, S. V. Patsaeva, J. Phys. Chem. A 119 (2015) 10806.

[8] L. Saiz, J. A. Padró, E. Guàrdia, J. Phys. Chem. B 101 (1997) 78.

[9] C. J. Benmore, Y. L. Loh, J. Phys. Chem. 112 (2000) 5877.

[10] F. Li, Z. Men, S. Li, S. Wang, Z. Li, C. Sun, Spectrochim. Acta, Part A 189 (2018) 621.

[11] S. Pothoczki, L. Pusztai, I. Bakó, J. Mol. Liq. 271 (2018) 571.

[12] O. Takahashi, M. P. Ljungberg, L. G. M. Pettersson, J. Phys. Chem. B 121 (2017) 11163.

[13] M. P. Ljungberg, I. Zhovtobriukh, O. Takahashi, L. G. M. Pettersson, J. Chem. Phys. 146 (2017) 134506.

[14] T. Tokushima, Y. Harada, O. Takahashi, Y. Senba, H. Ohashi, L. G. M. Pettersson, A. Nilsson, S. Shin, Chem. Phys. Lett. 460 (2008) 387.

[15] M. P. Ljungberg, Physical Review B 96 (2017) 214302.

[16] M. Haughney, M. Ferrario, I. R. McDonald, J. Phys. Chem. 91 (1987) 4934.

[17] B. Chen, J. I. Siepmann, J. Phys. Chem. B 110 (2006) 3555.

[18] J. Lehtola, M. Hakala, K. Hämäläinen, J. Phys. Chem. B 114 (2010) 6426.

# Chapter 5

# Identification of valence electronic states of liquid water

## 5-1 Introduction

As mentioned in Chapter 1-4, in the experimental XES of liquid water, the double peak structure appears around 525-526 eV [1]. The double peaks are assigned as $1b_1$' and $1b_1$", where $1b_1$' and $1b_1$" are MOs assigned as only one peak at $1b_1$ in gas phase [2]. The several interpretations of the double peaks are reported. One of them is based on a two-structure model, and another is a uniform, continuous liquid model. The two interpretations consistent with the importance of h-bonding but differ in the details of that interpretation. The two-structure model [3] claimed that the double peaks are due to the two different h-bonding structure, tetrahedral and distorted structure, shown in Figure 1-5. On the other hand, the uniform, continuous liquid model [4] claimed that the double peaks are due to the ultrafast O-H bond dissociation dynamics during the lifetime of the O 1s core hole.

In this Chapter, we report the theoretical reproduction of the double $1b_1$ peak feature of XES in liquid water. Several effects, such as geometry and dynamics, were discussed to determine the shape of the XES spectra.

## 5-2 The theoretical XES spectra of liquid water

Figure 5-1a shows the calculated XES spectra of liquid water from 270 to 360 K. The calculated spectra reproduced several features observed experimentally, as shown Figure 1-4. The double-peak feature of the $1b_1$ state observed in the experimental XES spectrum was successfully reproduced [3-5]. The XES spectrum calculated at low temperatures also resembles amorphous ice [3]. The calculated double $1b_1$ peaks are separated by approximately 0.9–1.1 eV depending on the temperature, which the experimental ones are reported as 0.7–0.9 eV [3] and 0.8 eV at the room temperature [5]. These values are slightly larger than the experimental values especially at high temperature region, probably because of the procedure used for the initial geometries and the electronic structure calculations [6]. The relative intensity of the $1b_2$ state to the $1b_1$ and $3a_1$ states increased with temperature. Focusing on the $1b_1$ peak profiles, the lower side peak ($1b_1$') was observed to be stable against increasing temperature, while the higher peak ($1b_1$") shifted to a higher energy, as shown in Figure 5-1b. The $1b_1$" peak intensity increased with increasing temperature. These features, which cannot be explained only by a simple two-state model, require other mechanisms such as density variation with temperature, which has already been discussed by Tokushima et al. [3]. Furthermore, the isotope dependence of the XES spectra of water at 300 K is shown in Figure 5-1c. The relative intensity of the $1b_1$' peak to the $1b_1$" peak is lower for $D_2O$, whereas it is higher for $H_2O$, suggesting that these differences call for a dynamical effect

on the core-hole state. To extract the XES profile without core-hole induced dynamics, the XES spectra for the sampled initial structure of liquid water without time evolution are shown in Figure 5-1d. The electronic states examined are single valence hole states, corresponding to those probed by ultraviolet photoelectron spectroscopy (UPS). Theoretically, a single $1b_1$ peak whose energy position corresponds to the XES $1b_1$" peak is obtained but with a narrower profile than the XES $1b_1$" peak. The simulated spectra are consistent with the experimental UPS spectra obtained by Winter et al. [7], and the spectral profile was stable against temperature. Therefore, the specific structure observed by XES may be indistinguishable by UPS. The second peak, assigned as $1b_1$', was reproduced by considering core-hole induced dynamics. However, the interpretation of the temperature dependence of XES is not straightforward.

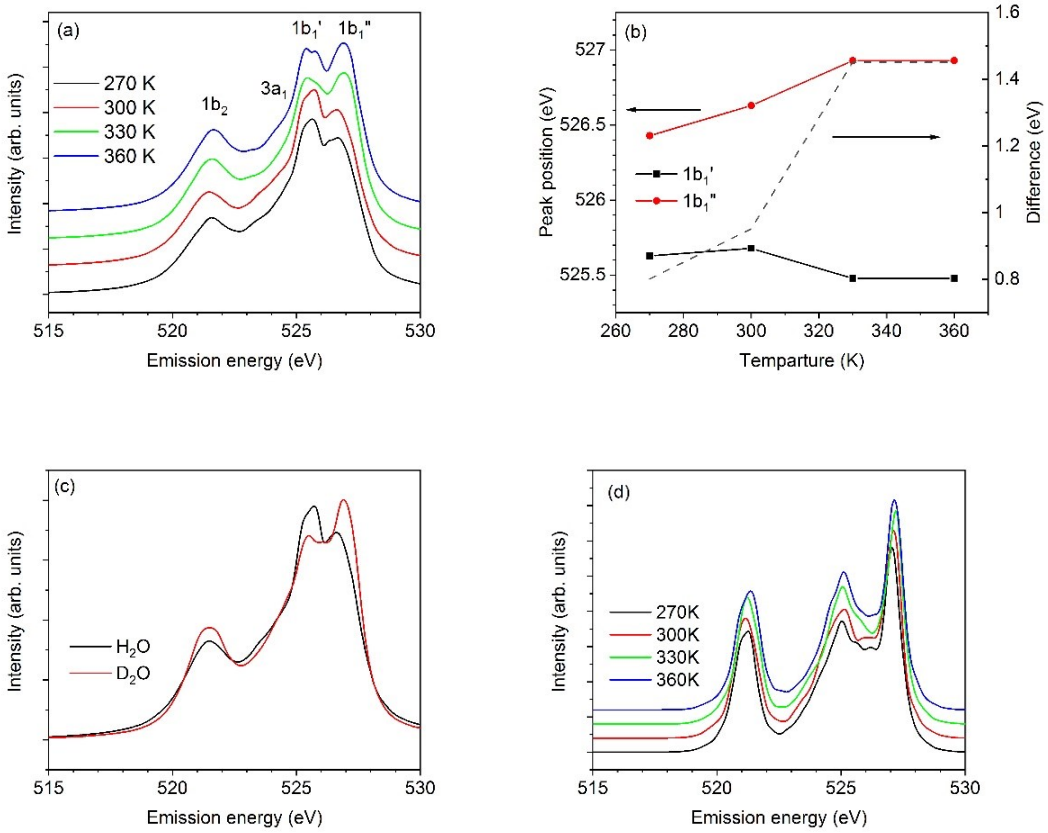


Figure 5-1: (a) Temperature dependence of theoretical XES spectra of water from 270 to 360 K including the effect of core-hole induced dynamics. Inset of this figure set magnified around peak top of $1b_1$ states. (b) Peak position of $1b_1$' and $1b_1$" states (solid lines) and these energy difference (dashed line) from 270 to 360 K. (c) Isotope dependence of theoretical XES spectra of water at 300 K including the effect of core-hole induced dynamics. (d) Temperature dependence of theoretical XES spectra of water from 270 to 360 K without core-hole induced dynamics.

## 5-3 Effect of local hydrogen bonding on XES spectra

To better understand the appearing features, the calculated spectra were classified into different types of h-bonds. The h-bonding criteria by Wernet et al. [8] were applied to examine the formation of h-bonding. In the present study, the XES spectra were simply classified by the number of h-bonding, i.e., H*m*, where *m* is the sum of the number of h-bonding donors and acceptors. In the present study, we did not distinguish h-bonding donors and acceptors to extract a simple picture related to the induced dynamics with a core hole. Figure 5-2a shows the XES spectra of water for several h-bonding types in 300 and 330 K. It is clear that the $1b_1$' peak appears for the H4 and H3 structures. The double peak features can be observed for all types of h-bonding. The $1b_1$' peak still more related to tetrahedral structures but not being a simple peak but also shifting a shoulder towards higher energy. In the case of fewer h-bonding, the intensity of the $1b_1$" peak is higher than that of the $1b_1$' peak, while the opposite is true in the case of four h-bonding. Figure 5-2b shows the h-bonding type distribution obtained by analyzing the geometries of the MD simulations. H4 and H2 correspond to a tetrahedrally coordinated cluster for a central water molecule and a distorted cluster, respectively. LDL and HDL include these local structures at different ratios. The main contribution is H3, which corresponds to the intermediate H-bond types between H2 and H4. For H1 and H2, the population increases monotonically with temperature. H3 and H4 display the opposite trend, while H5 has a minor contribution because the maximum coordination number of

a water molecule by the h-bonding should be four. The result is consistent with that of Miguel et al. [9] in terms of the h-bond distribution. It should be noted that the h-bonding distribution is directly reflected in the relative intensities of the $1b_1$' and $1b_1$" peaks in the XES spectra. In Figure 5-3, calculated XES spectra were classified into the type of h-bonding. The

spectrum of D2A2, which is presumed to be close to the ice structure, has the intensity of the $1b_1$', while the more peripheral D0A0, which is isolated from itself, has the intensity of $1b_1$".

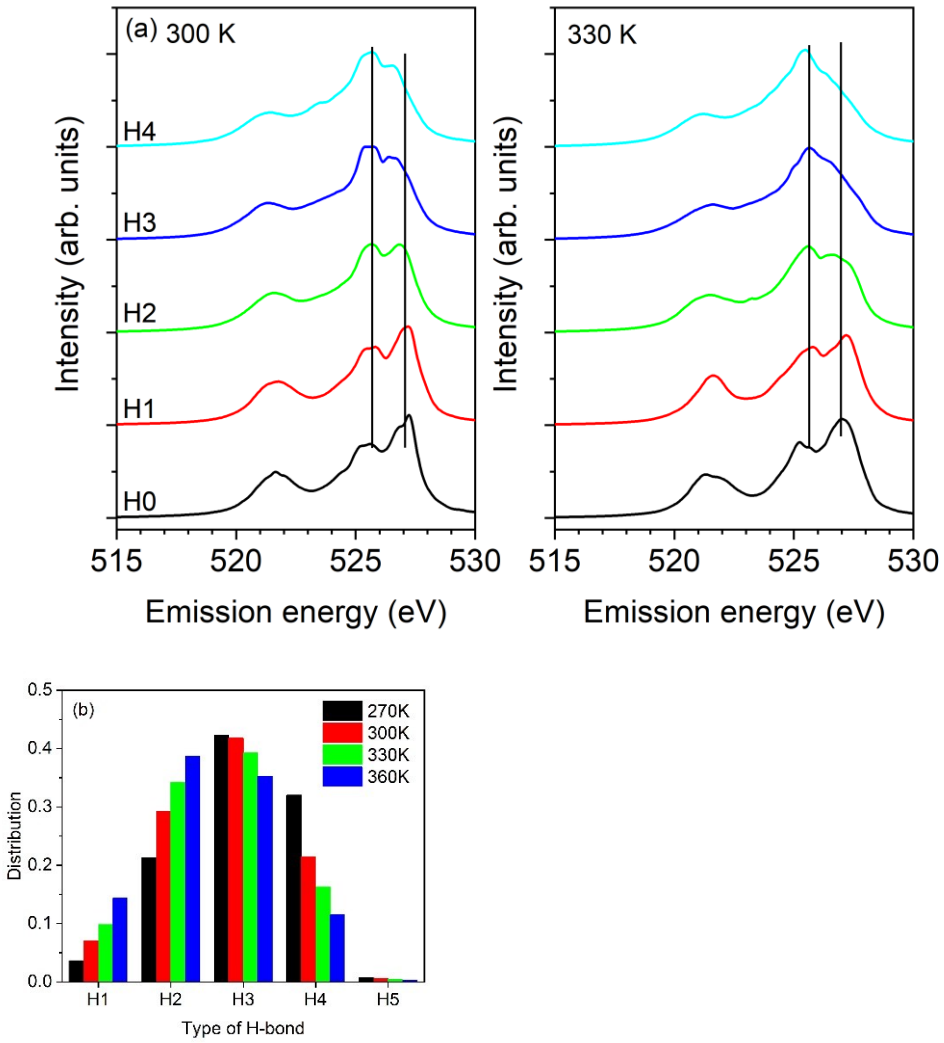


Figure 5-2: (a) Theoretical XES spectra of $H_2O$ depending the type of h-bonds in 300 and 330 K. H*m* means that numbers of h-bonds are *m*. (b) Distribution depending on the type of h-bond from 270 to 360 K.

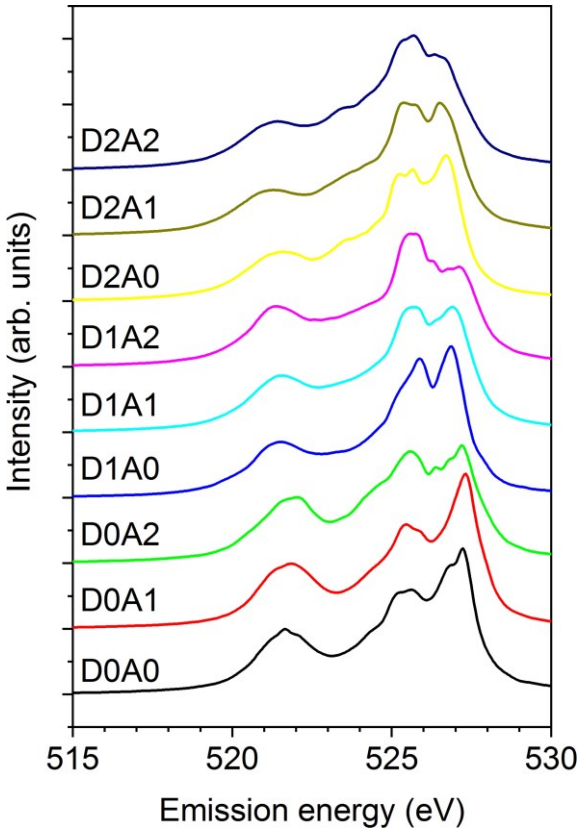


Figure 5-3: Theoretical XES spectra of $H_2O$ depending on the type of h-bonds which is classified by the number of h-bond donors and acceptors.

## 5-4 Effect of local hydrogen bonding on dynamics

Figure 5-4a shows the 20 fs propagation of the XES spectra for H4 at 300 K. The main features are similar, suggesting that the effect of the core-hole induced dynamics is similar among all the types of h-bonding. Figure 5-4 focused on the peak shift and intensity modulation of the $1b_1$ peak, which is stable for the first few femtoseconds after core excitation. It then starts to move toward lower energy, gradually decreasing in intensity. The rate of the highest peak position and intensity over time, as a function of the number of h-bonds, are plotted in Figure 5-4b. Except for the intensity decay of H1, increasing the number of h-bonds decreases both the rates, indicating that the increase in the number of h-bonds accelerates the core-hole induced dynamics, probably owing to the electrostatic field of the surrounding molecules. As shown in Figure 5-1c and d, the isotope effect and the absence of temperature effect without core-hole induced dynamics show the influence of core-hole induced hydrogen atom dynamics on the XES spectra. The peak shift of the $1b_1$ state is suppressed by increasing the mass from hydrogen to deuterium, causing an increase in the $1b_1$'' peak, as observed in previous studies [3,4].

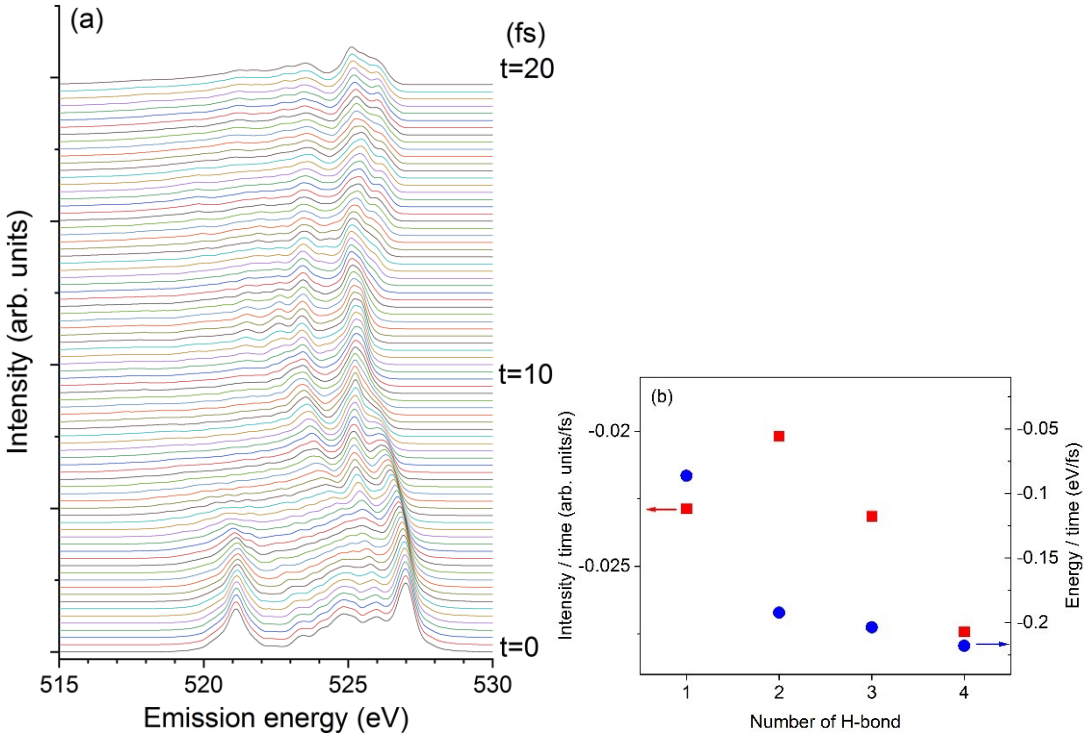


Figure 5-4: (a) Time propagation of theoretical XES spectra at 300 K for the case of H4 during 20 fs. (b) Rate of highest peak position (blue circle) and the intensity (red square) over time as a function of the number of h-bonds.

## 5-5 Effect of vibration on XES spectra

Next, to examine the effect of thermally excited vibrational modes on the XES spectra. In the previous study, Zhovtobriukh et al. included thermal effects to simulate the XES spectra of liquid water by incorporating two O-H stretch modes [10]. These two vibrational modes should be sufficient for describing the effect of h-bond dynamics because they have a much deeper potential energy surface than the other modes. In the present study, the effects of the other modes on the XES spectra are discussed. For a water molecule in a liquid, more than three internal modes can be obtained: Anti-symmetric and symmetric O-H stretching, bending, three rotational, and three translational modes. The latter six modes were assigned as intermolecular modes. By optimizing the geometry of the central water molecule, we obtained nine independent vibrational modes and examined their effects on the XES spectra using the SCKH scheme [11]. The results at 300 K are summarized in Figure 5-5. As discussed above, the effects of core-hole induced dynamics are similar. Instead, the difference is whether excited vibrational modes are along the h-bond direction. Since motion along the direction of the h-bonds is expected to accelerate the peak shift, the deviation from the O-H bond direction, including the core-excited oxygen atom, should influence the spectra more effectively. When the O-H stretching modes are excited, core-hole induced hydrogen atom dynamics along the O-H bond line are accelerated, which increases the $1b_1$' peak. However, exciting the vibrational modes that move the hydrogen atom perpendicular

to the line of the O-H bond suppresses the core-hole induced dynamics, decreasing the $1b_1$' peak. This mode sensitivity to the XES $1b_1$ profile may depend on the depth of the potential energy surface of the O-H stretching mode.

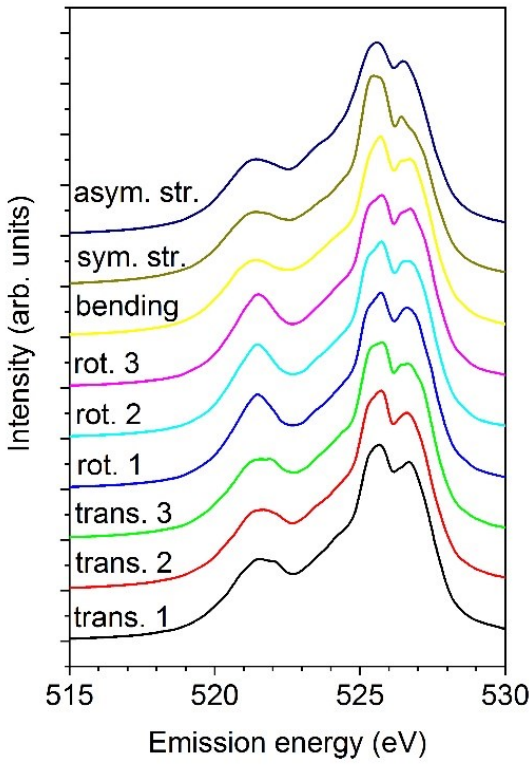


Figure 5-5: Theoretical XES spectra for each vibrational mode at 300 K. The spectra are stacked as increasing the vibrational number. "asym. str." and "sym. str." mean anti-symmetric and symmetric stretching modes.

## 5-6 Factors affecting XES spectra of liquid water

The key parameters determining the XES $1b_1$ profile are the density of water and the orientation of water molecules surrounding the core-excited water molecule as a function of the temperature. In liquid water, the decrease in the density of water, arising from an increase in its temperature from 4 °C at maximum density, may produce less effective core-hole induced dynamics, as discussed in Figure 5-4b, and contributes to the increase of the $1b_1$" peak at higher temperatures. However, when the temperature is decreased from 4 °C, the influence of the density of water is dominated by other effect, namely, the alignment of hydrogen bonds along the O-H bond axis direction, as evident from the increase in the four-coordinate h-bonding, shown in Figure 5-2b. This effect accelerates the core-hole induced dynamics, and the $1b_1$' peak should dominate. Therefore, the relative intensity between the $1b_1$' and $1b_1$" peaks may be sensitive to various physical properties, such as the local density around the excited water molecule, number of h-bonding, and the h-bonding orientational distribution.

## 5-7 Conclusion

The XES spectra of liquid water were successfully reproduced by incorporating the effects of perfect vibrational modes, O-H stretching, bending, and rotation modes. Both temperature and isotope dependence were accounted for by considering the h-bonding configurations around the excited water molecules and the dynamics induced by the core holes. The current procedure is generalized and may be applied to future studies of aqueous conditions. Several problems remain. In particular, the reproducibility of the splitting energies of the $1b_1'$ and $1b_1''$ peaks is consistent with experiments at room temperature, but not at elevated temperatures. These could be further refined by accurate theoretical calculations of both the geometry sampling and the electronic structure using more sophisticated procedures.

## References


[1] A. Nilsson, D. Nordlund, I. Waluyo, N. Huang, H. Ogasawara, S. Kaya, U. Bergmann, L. A. Naslund, H. Ostrom, P. Wernet, K.J. Andersson, T. Schiros, L. G. M. Pettersson, J. Electron. Spectrosc. Relat. Phenom. 177 (2010) 99.

[2] T. Tokushima, Y. Horikawa, H. Arai, Y. Harada, O. Takahashi, L. G. M. Pettersson, A. Nilsson, S. Shin, J. Chem. Phys. 136 (2012) 044517.

[3] T. Tokushima, Y. Harada, O. Takahashi, Y. Senba, H. Ohashi, L. G. M. Pettersson, A. Nilsson, S. Shin, Chem. Phts. Lett. 460 (2008) 387.

[4] O. Fuchs, M. Zharnikov, L. Weinhardt, M. Blum, M. Weigand, Y. Zubavichus, M. Bar, F. Maier, J. D. Denlinger, C. Heske, M. Grunze, E. Umbach, Phys. Rev. Lett. 100 (2008) 027801.

[5] K. Yamazoe, J. Miyawaki, H. Niwa, A. Nilsson, Y. Harada, J. Chem. Phys. 150 (2019) 204201.

[6] O. Takahashi, L. G. M. Pettersson, J. Chem. Phys.121 (2004) 10339.

[7] B. Winter, R. Weber, W. Widdra, M. Dittmar, M. Faubel, I. V. Hertel, J. Phys. Chem. A 108 (2004) 2625.

[8] P. Wernet, D. Nordlund, U. Bergmann, M. Cavalleri, M. Odelius, H. Ogasawara, L. A. Naslund, T. K. Hirsch, L. Ojamae, P. Glatzel, L. G. M. Pettersson, A. Nilsson, Science 304 (2004) 995.

[9] B. Miguel, J. Zúñiga, A. Requena, A. Bastida, J. Phys. Chem. B 118 (2014) 9427.

[10] I. Zhovtobriukh, N. A. Besley, T. Fransson, A. Nilsson, L. G. M. Pettersson, J. Chem. Phys. 148 (2018) 144507.

[11] M. P. Ljungberg, A. Nilsson, L. G. M. Pettersson, Physical Review B 82 (2010) 245115.

# Chapter 6

# Summary and future work

In this thesis, the theoretical and experimental studies of liquid structure using soft x-rays are presented. First, experimental soft x-ray spectra of oxalic acid, the simplest dicarboxylic acid, in aqueous solution were theoretically reproduced. The spectra of reflect properties that are not present in the monocarboxylic acetic acid, indicating that it can be adapted for use in more complex molecules. Soft x-ray experiments require a high intensity light source, which limits the number of places where such experiments can be conducted. Therefore, it is expected to obtain information via soft x-rays without experiments by using chemical informatics (CI), which has attracted attention in recent years. However, in order to perform CI, information on the emission from basic functional groups is necessary, but this information is still lacking. By using this technique for other simple molecules, we obtain information on the electronic state and the structure of molecules in liquids.

Soft x-ray spectroscopy has been considered an important tool for advancing the analysis of the structure of liquids, but the interpretation of its spectra has long been divided. In this thesis, by combining experiments and theoretical calculations in liquid ethanol and water, we showed that the hydrogen bonding structure has a significant effect on the spectrum. It was

also shown that the h-bonding structure has a significant effect on the relaxation dynamics after excitation. We analyzed h-bonding in a single component, but in many cases, liquids are mixed with other substances and interact with them. In the future, we will work on the analysis of hydrogen bonding in mixtures.

## Acknowledgments

The present works were carried out at Department of Chemistry, Graduate School of Science, Hiroshima University, under the supervision of Professors Osamu Takahashi. The synchrotron radiation experiments were performed on the BL17SU and BL07SUL at SPring-8. We would like to thank the Research Center for Computational Science, Okazaki, Japan for use of their Fujitsu PRIMERGY system, and the Research Institute for Information Technology at Kyushu University, Fukuoka, Japan for use of their HITACHI HA8000-tc system.

First of all, I would like to express my deep gratitude to Professor Takahashi for his dedicated instructions for as long as 5 years. I am also deeply grateful to the professors who guided me at Department of Chemistry, and School of Integrated Arts and Sciences, Hiroshima University. Especially, I am deeply grateful to Professor Akihiko Toda, who is the supervision in undergraduate school.

The authors would also like to thank Dr. Takashi Tokushima at Lund University, Professor Yoshihisa Harada at Tokyo University, Dr. Kosuke Yamazoe at ISSP, Dr. Jun Miyawaki at QST, Professor Yuka Horikawa at Yamaguchi University and Dr. Masaki Oura at RIKEN for experimental measurements, Professor Lars Pettersson for theoretical advises. I would like to thank the people who have supported my research. Especially, I would like to thank the members of the laboratory of structural physical chemistry, in

Japanese, kouzoubutsurikagaku, Professor Takayuki Ebata, Professor Yoshiya Inokuchi, Professor Satoru Muramatsu, Taiga Suenaga, Takashi Koga, Nozomu Futamata, Kento Akihiro, Shotaro Yamaguchi, Kyoko Ito, Takuma Ohnishi, Shin-nosuke Kinoshita, and Motoki Kida.

Finally, I sincerely thank my friends and family, who are always my spiritual supports.

Ryosuke Yamamura